

# Spatio-Temporal Big Data Analysis for Smart Grids Based on Random Matrix Theory: A Comprehensive Study

Robert Qiu<sup>1,2,3</sup>, Lei Chu<sup>2,3</sup>, Xing He<sup>2,3</sup>, Zenan Ling<sup>2,3</sup>, Haichun Liu<sup>2,3</sup>

<sup>1</sup>Tennessee Technological University, Cookeville, TN 38505 USA.

<sup>2</sup>Department of Electrical Engineering, Shanghai Jiaotong University, Shanghai 200240, China.

<sup>3</sup>Research Center for Big Data Engineering and Technology, State Energy Smart Grid Research and Development Center.

## Abstract

A cornerstone of the smart grid is the advanced monitorability on its assets and operations. Increasingly pervasive installation of the phasor measurement units (PMUs) allows the so-called synchrophasor measurements to be taken roughly 100 times faster than the legacy supervisory control and data acquisition (SCADA) measurements, time-stamped using the global positioning system (GPS) signals to capture the grid dynamics. On the other hand, the availability of low-latency two-way communication networks will pave the way to high-precision real-time grid state estimation and detection, remedial actions upon network instability, and accurate risk analysis and post-event assessment for failure prevention.

In this chapter, we firstly modelling spatio-temporal PMU data in large scale grids as random matrix sequences. Secondly, some basic principles of random matrix theory (RMT), such as asymptotic spectrum laws, transforms, convergence rate and free probability, are introduced briefly in order to the better understanding and application of RMT technologies. Lastly, the case studies based on synthetic data and real data are developed to evaluate the performance of the RMT-based schemes in different application scenarios (i.e., state evaluation and situation awareness).

## Index Terms

Spatio-Temporal Data, Big Data, Random Matrix Theory, Smart Grids.

## I. INTRODUCTION

### A. Perspective on Smart Grids

The modern power grid is one of the most complex engineering systems in existence; the North American power grid is recognized as the supreme engineering achievement in the 20th century [1]. The complexity of the future's electrical grid is ever increasing: 1) the evolution of the grid network, especially the expansion in size; 2) the penetration of renewable/distributed resources, flexible/controllable electronic units, or even prosumers with dual load-generator behavior [2]; and 3) the revolution of the operation mechanism, e.g. demand-side management. Also, the financial, the environmental and the regulatory constraints are pushing the electrical grid towards its stability limit.

Generally, power grids have experienced three ages—G1, G2, and G3 [3]. The network structures are depicted in Fig. 1 [4]. Their data flows and energy flows, as well as corresponding data management systems and work modes, are quite different [5], which are shown in Fig. 2 and Fig. 3, respectively.

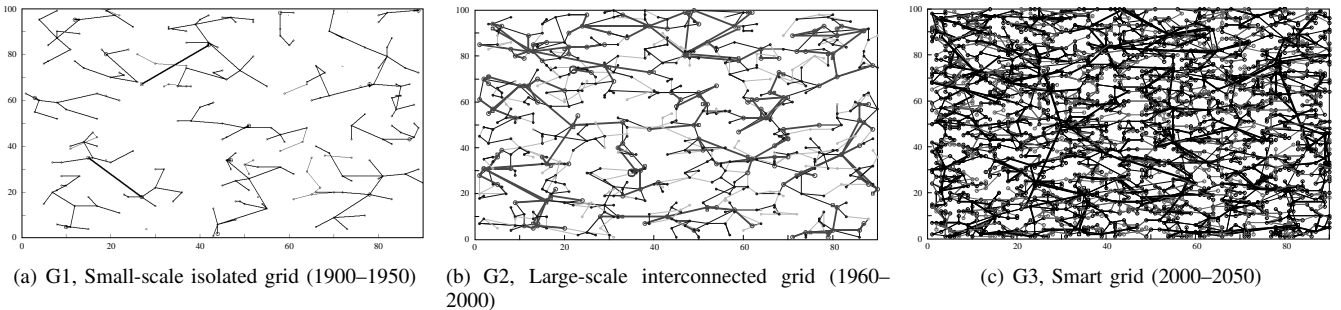


Fig. 1. Topologies of Grid Network.

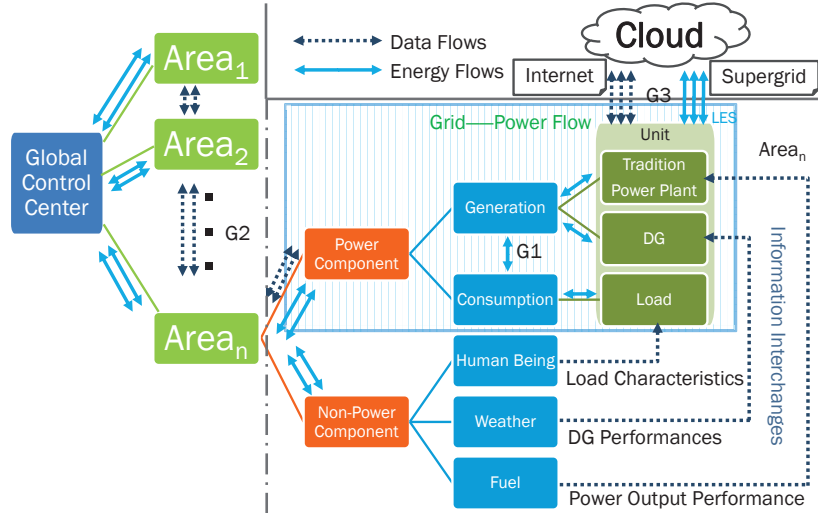


Fig. 2. Data flows and energy flows for three generations of power systems. The single lines, double lines, and triple lines indicate the flows of G1, G2, and G3, respectively.

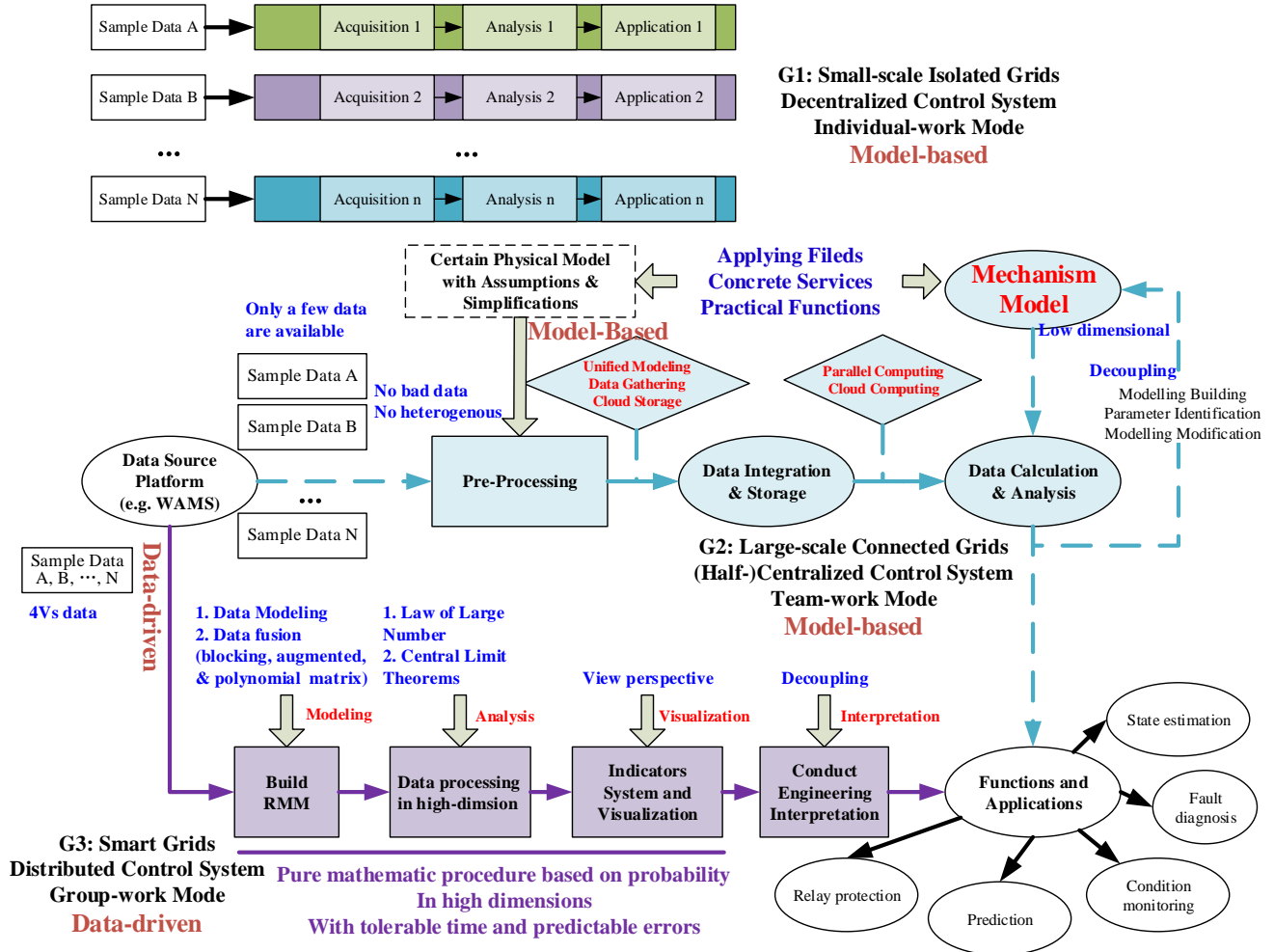


Fig. 3. Data management systems and work modes for three ages of power systems. The above, middle, and below parts indicate the data management systems and the work modes of G1, G2, and G3, respectively. For G1, each grid works independently. For G2, global and local control centers are operating under the team-work mode. For G3, the group-work mode breaks through the regional limitation for energy.

### **G1 : Small – scale isolated grids**

G1 was developed from power system around 1900 to 1950, featured by small-scale isolated grids. For G1, units interchange energy and data within the isolated grid to keep generation-consumption balance. The units are most controlled by themselves, i.e., operating under individual-work mode. As shown in Fig. 1(a), each apparatus collects designated data, and makes corresponding decisions only with its own application. The individual-work mode works with an easy logic and little information communication. However, it means few advanced functions and inefficient utilization of resources. It is only suitable for small grids or isolated islands.

### **G2 : Large – scale interconnected grids**

G2 was developed from power grids about 1960 to 2000, featured by zone-dividing large-scale interconnected grids. For G2, units interchange energy and data with the adjacent ones. The units are dispatched by a control center, i.e. operating under team-work mode. The regional team leaders, such as local dispatching centers, substations, and microgrid control centers, aggregate their own team-members (i.e. units in the region) into a standard black-box model. These standard models will be further aggregated by the global control center for control or prediction purposes. The two aggregations above are achieved by four steps: data monitoring, data pre-processing, data storage, and data processing. The description above can be summarized by dotted blue lines in Fig. 3. In general, the team-work mode conducts model-based analysis, and mainly concerns system stability rather than individual benefit; it does not work well for smart grids with 4Vs data.

### **G3 : Smart grids**

The development of G3 was launched at the beginning of the 21st century; and for China, it is expected to be completed around 2050 [3]. Fig. 1(c) shows that the clear-cut partitioning is no longer suitable for G3, as well as the team-work mode which is based on the regional leader. For G3, the individual units, rather than the regional center (if still exists), play a dominant role. They are well self-control with high intelligence, resulting in much more flexible flows for both energy exchange and data communication [6]. Accordingly, the group-work mode is proposed. Under this mode, the individuals freely operate under the supervision of the global control centers [5]. VPPs [7], MMGs [8], for instance, are typically G3 utilities. These group-work mode utilities provide a relaxed environment to benefit both individuals and the grids: the former (i.e. individuals), driven by their own interests and characteristics, are able to create or join a relatively free group to benefit mutually from sharing their own superior resources; meanwhile, these utilities are often big and controllable enough to be good customers or managers to the grids.

## ***B. The Role of Data in Future Power Grid***

Data are more and more easily accessible in smart grids. Fig. 4 shows numerous data sources: Information Communication Technology (ICT), Advanced Metering Infrastructure (AMI), Supervisory Control and Data Acquisition (SCADA), Sensor Technology (ST), Phasor Measurement Units (PMUs), and Intelligent Electronic Devices (IEDs) [9]. Hence, data with features of volume, velocity, variety, and veracity (i.e. 4Vs data) [10] are inevitably generated and daily aggregated. Particularly, the "4Vs" are elaborated as follows:

- *Volume*. There are massive data in power grids. The so-called curse of dimensionality [11] occurs inevitably. The world wide small-scale roof-top photovoltaics (PVs) installation reached 23 GW at the end of 2013, and the growth is predicted to be 20 GW per year until 2018. The up-take of electric vehicles (EVs) also continues to grow. At least 665,000 electric-drive light-duty vehicles, 46,000 electric buses and 235 million electric two-wheelers were in the worldwide market in early 2015 [12].
- *Velocity*. The resource costs (time, hardware, human, etc.) for big data analytics should be tolerable. To sever on-line decision-makings, massive data must be processed within a fraction of second.
- *Variety*. The data in various formats are often derived from diverse departments. In the view of data management, sampling frequency of source data, processing speed and service objects are not completely accord.
- *Veracity*. For a massive data source, there often exist realistic bad data, e.g. incomplete, inaccurate, asynchronous, and unavailable. For system operations, decisions such as protection, should be highly reliable.

As mentioned above, smart grids are always huge in size and complex in topology; big data analytics and data-driven approach become natural solutions for the future grid [13–16]. Driven by data analysis in high-dimension, big data technology works out data correlations (indicated by statistical parameters) to gain insight to the inherent mechanisms. Actually, big data technology has already been successfully applied as a powerful data-driven tool for numerous phenomena, such as quantum systems [17], financial systems [18, 19], biological systems [20], as well as wireless communication networks [21–23]. For smart grids, data-driven approach and data utilization are current stressing topics, as evidenced in the special issue of "Big Data Analytics for Grid Modernization" [24]. This special issue is most relevant to our book in spirit. Several SA topics are discussed as well. We highlight anomaly detection and classification [25, 26], social media such as Twitter in [27], the estimation of active ingredients such as PV installations [28, 29] and finally the real-time data for online transient stability evaluation [30]. In addition, we point out researchs about the improvement in wide-area monitoring, protection and control (WAMPAC) and the utilization of PMU data [31–34], together with the fault detection and location [35–37]. Xie et al., based on Principal component analysis (PCA), proposes an online application for early event detection by introducing a reduced dimensionality [38]. Lim et

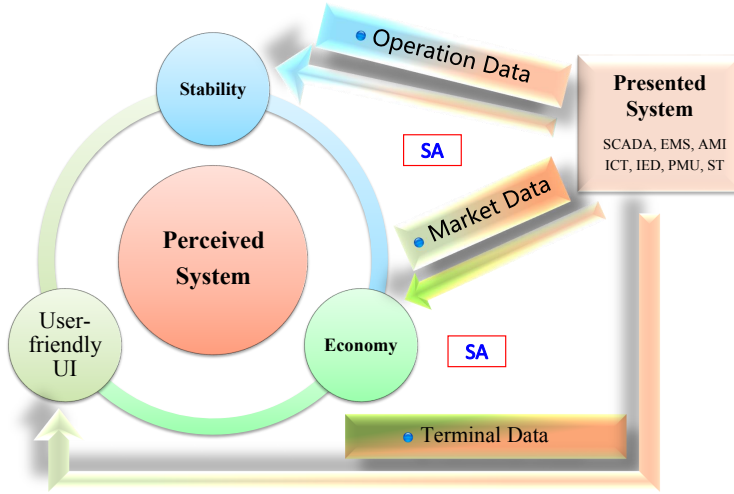


Fig. 4. Smart grid with 4Vs data and its SA.

al. studies the quasi-steady-state operational problems relevant to the voltage instability phenomena [39]. These works provide primary exploration of the big data analysis in smart grid. Furthermore, a brief account for random matrix theory (RMT) which can be seen as basic analysis tools for spatial-temporal grid data processing, is elaborated in the following subsection.

### C. A Brief Account for RMT

The last two decades have seen the rapid growth of RMT in many science fields. The brilliant mathematical works in RMT shed light on the challenges from classical statistics. In this subsection, we present a brief introduction to the main development of the RMT. The application-related account, with particular attention paid to recently rising RMT-based technology that are relevant for smart grid, is elaborated in Section III.

The research of random matrices began with the work of Wishart in 1928 which focused on the distribution of the sample covariance matrices. The first asymptotic results on the limit spectrum of large random matrices (energy levels of nuclei) were obtained by Wigner in 1950s in a series of works [40–43] which ultimately lead to the well-known Semi-Circle Law [44]. Another breakthrough was presented in [45] that studied the distribution of eigenvalues for empirical covariance matrices. Based on these excellent works, RMT became a vibrant research direction of its own. Plenty of brilliant works that branched off the early physical and statistical applications were put forward in the last decades. For the sake of brevity, here we only show two remarkable results that turned out to be related to a large number of research hotspots in economics, communications and smart grid. One of the most striking progress is the discovery of the Tracy Widom distribution of extreme eigenvalues and another one is the single ring law which described the limit spectrum of eigenvalues of non-normal square matrices [46]. Interested readers are referred to monographs [47–49] for more details.

We will end this section by providing the structure of the remainder of this chapter.

Firstly, Section II gives a tutorial account of existing mathematical works that are relevant to the statistical analysis of random matrices arising in smart grids. Specially, Section II-A introduces data collected from the widely applied phasor measurement unit and data modelling using linear and nonlinear combination of random matrices. Section II-B focuses on asymptotic spectrum laws of the major types of random matrices. Section II-C presents some three dominant transforms which play key roles in describing the limit spectra of random matrices. Recent results on the convergence rate to the asymptotic limits are contained in the Section II-D. Section II-E is dedicated to the free probability theory which is demonstrated as a practical tool for smart grids.

Secondly, we begin with some representative problems arisen from widely deployment of synchronous phasor measurement units that capture various features of interest in smart grids. We then show how random matrix theories have been used to characterize the data collected from synchronous phasor measurement and tackle the problems in the era of "Big Data". In particular, Section III-A provides some basis hypothesis tests that remain fundamental to research into the behaviour of the data in smart grids. Section III-B concerns stability assessment from some recently developed data driven methods that based on RMT. Section III-C focuses on situation awareness for smart grids from linear eigenvalue statistics. Early event detection problem is studied in details using free probability in Section III-D.

## II. RMT: A PRACTICAL AND POWERFUL BIG DATA ANALYSIS TOOL

In this section, we provide a comprehensive existing mathematical results that are associated with the analysis of statistics of random matrices arising in smart grid. We also describe some new results on random matrices and other data-driven methods which were inspired by problems of engineering interest.

### A. Modelling Grid Data using Large Dimensional Random Matrices

Before the comprehensive utilization of RMT framework, we try to build a model for spatio-temporal PMU data using large dimensional random matrices.

It is well accepted that the transient behavior of a large electric power system can be illustrated by a set of differential and algebraic equations (DAEs) as follows [50]:

$$\dot{\mathbf{x}}^{(t)} = \mathbf{f}(\mathbf{x}^{(t)}, \mathbf{u}^{(t)}, \mathbf{h}^{(t)}, w) \quad (1)$$

$$0 = \mathbf{g}(\mathbf{x}^{(t)}, \mathbf{u}^{(t)}, \mathbf{h}^{(t)}, w) \quad (2)$$

where  $\mathbf{x}^{(t)} \in \mathbb{C}^{m \times p}$  are the power state variables, e.g., rotor speeds and the dynamic states of loads,  $\mathbf{u}^{(t)}$  represent the system input parameters,  $\mathbf{h}^{(t)}$  define algebraic variables, e.g., bus voltage magnitudes,  $w$  denote the time-invariant system parameters.  $t \in \mathcal{R}$ ,  $m$  and  $p$  are the sample time, number of system variables and bus, respectively. The model-based stability estimators [51, 52] focus on linearization of nonlinear DAEs in (1) and (2) which gives

$$\begin{bmatrix} \Delta \dot{\mathbf{x}} \\ \Delta \dot{\mathbf{u}} \end{bmatrix} = \begin{bmatrix} \mathbf{A} & -\mathbf{f}_{\mathbf{u}} \mathbf{g}_{\mathbf{u}}^{-1} \mathbf{g}_{\mathbf{h}} \\ \mathbf{0} & -\mathbf{E} \end{bmatrix} \begin{bmatrix} \Delta \mathbf{x} \\ \Delta \mathbf{u} \end{bmatrix} + \begin{bmatrix} \mathbf{0} \\ \mathbf{C} \end{bmatrix} \xi, \quad (3)$$

where  $\mathbf{f}_{\mathbf{x}}$ ,  $\mathbf{f}_{\mathbf{u}}$  are the Jacobian matrices of  $\mathbf{f}$  with respect to  $\mathbf{x}$ ,  $\mathbf{u}$  and  $\mathbf{A} = \mathbf{f}_{\mathbf{x}} - \mathbf{f}_{\mathbf{u}} \mathbf{g}_{\mathbf{u}}^{-1} \mathbf{g}_{\mathbf{x}}$ .  $\mathbf{E}$  is a diagonal matrix whose diagonal entries equal  $t_{cor}^{-1}$  and  $t_{cor}$  is the correction time of the load fluctuations.  $\mathbf{C}$  denotes a diagonal matrix whose diagonal entries are nominal values of the corresponding active ( $P$ ) or reactive ( $Q$ ) of loads;  $\xi$  is assumed to be a vector of independent Gaussian random variables.

It is noted that estimating the system stability by solving the equation (3) is becoming increasingly more challenging [49] as a consequence of the steady growth of the parameters, say,  $t$ ,  $p$  and  $m$ . Besides, the assumption that  $\xi$  follows Gaussian distribution would restrict the practical application.

On the other hand, as a novel alternative, the lately advanced data driven estimators [38, 39, 52, 53] can assess stability without knowledge of the power network parameters or topology. However, these estimators are based on the analysis of individual window-truncated PMU data. In this chapter, we seek to provide a method with ability of continuous learning of power system from spatio-temporal PMU data.

Firstly, we provide a novel method for modelling the spatio-temporal PMU data. Fig. 5 illustrates the conceptual representation of the structure of the spatio-temporal PMU data. More specifically, let  $p$  denote the number of the available PMUs across the whole power network, each providing  $c$  measurements. At  $i$ th time sample, a total of  $\kappa = p \times c$  measurements, say  $\mathbf{z}_i$ , are collected. With respect to each PMU, the  $c$  measurements could contain many categories of variables, such as voltage magnitude, power flow and frequency, etc. In this chapter, we develop PMU data analysis assuming each type of measurements is independent. That is, we assume that at each round of analysis,  $\kappa := p$ . Given  $q$  time periods of  $T$  seconds with  $K$  Hz sampling frequency in  $k$ th data collection. Let  $n_g = T \times K$  and  $\mathbf{Z}_{ig} = \{\mathbf{z}_{i1}, \dots, \mathbf{z}_{in_g}\}$ ,  $i = 1, 2, \dots, n$ , a sequence of large random matrix

$$\left\{ \underbrace{\mathbf{Z}_{11}, \mathbf{Z}_{12}, \dots, \mathbf{Z}_{1q}}_{q \text{ window-truncated data}}, \dots, \underbrace{\mathbf{Z}_{n1}, \mathbf{Z}_{n2}, \dots, \mathbf{Z}_{nq}}_{q \text{ window-truncated data}} \right\} \quad (4)$$

is obtained to represent the collected voltage PMU measurements.

As illustrated in Fig. 5,  $\mathbf{Z}_i$  is a large random matrix with independent identical distributed entries. Here we also include other forms of basic random matrices that are relevant to the applications in smart grids as follows.

**Gaussian Unitary Ensemble (GUE):** Let  $\mathbf{Y}$  be  $N \times N$  Wigner matrix or so called Gaussian unitary ensemble GUE, and  $\mathbf{Y} = \{w_{ij}\}_{1 \leq i, j \leq N}$ .  $\mathbf{Y}$  satisfies the following conditions:

- 1) The entries of  $\mathbf{Y}$  are i.i.d Gaussian variables.
- 2) For  $1 \leq i \leq j \leq N$ ,  $\text{Re}(Y_{ij})$  and  $\text{Im}(Y_{ij})$ , are i.i.d. with distribution  $N(0, \frac{1}{2}\sigma^2)$ .
- 3) For any  $i, j$  in  $\{1, 2, \dots, N\}$ ,  $Y_{ij} = \bar{Y}_{ji}$ .
- 4) The diagonal entries of  $\mathbf{Y}$  are real random variable with distribution  $N(0, \sigma^2)$ .

For the convenience of analysis, we can denote GUE as  $\mathbf{Y} = \frac{1}{2}(\mathbf{X} + \mathbf{X}^H)$ . Besides, the joint p.d.f. of ordered eigenvalues of GUE ( $\lambda_1 \geq \lambda_2 \geq \dots \geq \lambda_N$ ) is [54, 55]

$$2^{-N/2} \pi^{-N^2/2} \exp \left[ -\frac{\text{Tr} \mathbf{Y}^2}{2} \right] \quad (5)$$

**Laguerre Unitary Ensemble (LUE):** Let  $\{X_{ij}\}_{1 \leq i \leq M, 1 \leq j \leq N}$  be i.i.d. Gaussian random variables with  $\mathbb{E}(X_{ij}) = 0$  and  $\mathbb{E}X_{ij}^2 = \frac{1}{2}(1 + \delta_{ij})$ . The so called Wishart matrix or Laguerre unitary ensemble LUE can be expressed as  $\mathbf{W} = \frac{1}{N} \mathbf{X} \mathbf{X}^H$ . The p.d.f. of  $\mathbf{W}$  for  $N \geq M$  is [47, 55]

$$\frac{\pi^{-M(M-1)/2}}{\det \sum \prod_{i=1}^M (N-i)!} \exp[-\text{Tr} \{\mathbf{W}\}] \det \mathbf{W}^{N-M}. \quad (6)$$

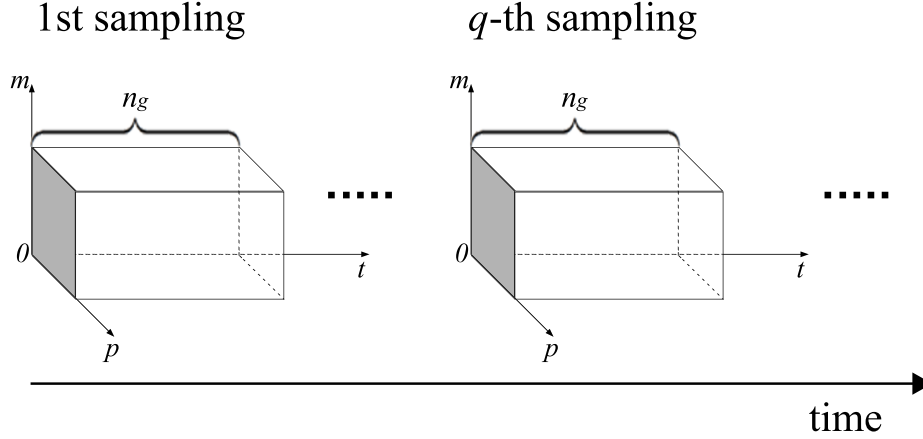


Fig. 5. Conceptual representation of the structure of the spatio-temporal PMU data.

### Large random matrix polynomials:

$$\mathbf{M} = f(\mathbf{A}) + g(\mathbf{B}),$$

where  $f, g$  are analytical functions,  $\mathbf{A}$  is GUE, and  $\mathbf{B}$  is LUE. See more details in Section II-E.

### B. Asymptotic Spectrum Laws

In this subsection, we provide a brief introduction to the asymptotic spectrum laws of the large basic random matrices as shown in the Section II-A. There are remarkable results describing the asymptotic spectrum laws. Here special attention is paid to the limit behavior of marginal eigenvalues as the data dimensions tend to infinity.

We start with the GUE matrix  $\mathbf{X} \in \mathbb{R}^N$  whose entries are independent identical distributed zero-mean (real or complex) Gaussian ensembles. As shown in [47], as  $N \rightarrow \infty$ , the empirical distribution of eigenvalues of  $\frac{1}{\sqrt{N}}\mathbf{X}$  converges to the well-known semi-circle law whose density can be represented as

$$\rho(\lambda) = \begin{cases} \frac{1}{2\pi} \sqrt{4 - \lambda^2} & \text{if } |\lambda| \leq 2 \\ 0 & \text{if } |\lambda| > 2 \end{cases} \quad (7)$$

Also shown in [40], the same result could be obtained for a symmetric  $\mathbf{X}$  whose diagonal entries are 0 and whose lower-triangle entries are independent and take the values  $\pm 1$  with equal probability.

If no attempt is made to symmetrize the square matrix  $\mathbf{X}$ , then the eigenvalues of  $\frac{1}{\sqrt{N}}\mathbf{X}$  are asymptotically uniformly distributed on the unit circle of the complex plane. This is referred as the well-known Grikko circle law which is elaborated in the following Theorem.

**Theorem II.1** (Circular Law [48]). *Let  $\xi$  be a complex random variable with mean zero and unit variance. For each  $N \geq 1$ . Let  $\mathbf{X}_N$  be an iid random matrix of size  $N$  with atom variable  $\xi$ . Then, for any bounded and continuous function  $f: \mathbb{C} \rightarrow \mathbb{C}$ ,*

$$\int_{\mathbb{C}} f(z) d\mu_{\frac{1}{\sqrt{N}}\mathbf{X}_N}(z) \rightarrow \frac{1}{\pi} \int_{\mathbb{U}} f(z) d^2 z$$

*almost surely as  $N \rightarrow \infty$  where  $\mathbb{U}$  is the unit disk in the complex plane  $|z| \leq 1$  and  $d^2 z = dx dy$ , with  $z = x + iy$ .*

Semi-circle law and Circular Law explain the asymptotic property of large random matrices with independent entries. However, as illustrated in Section I-B, the key issues in smart grid involve the singular values of rectangle large random matrix  $\mathbf{W} \in \mathbb{R}^{N \times T}$ . The LUE matrices  $\mathbf{W} = \frac{1}{T} \mathbf{Y}^H \mathbf{Y}$  have dependent eigenvalues of interest even if  $\mathbf{Y}$  has independent entries. Let the matrix aspect ratio  $c = T/N$ , the asymptotic theory of singular values of  $\mathbf{W}$  was presented by the landmark work [45] as follows.

As  $N, T \rightarrow \infty$  and  $c \leq 1$ , the limit distribution of the eigenvalues of  $\mathbf{W}$  converges to the so-called Marcenko-Pastur law whose density function is

$$\rho(\lambda) = \left(1 - \frac{1}{c}\right)^+ \delta(\lambda) + \frac{\sqrt{(\lambda - a)^+(b - \lambda)^+}}{2\pi c \lambda}, \quad (8)$$

where  $(x)^+ = \max(0, x)$  and

$$a = (1 - \sqrt{c})^2, b = (1 + \sqrt{c})^2$$

Analogously, when  $c \geq 1$ , the limit distribution of the eigenvalues of  $\mathbf{W}$  converges to

$$\tilde{\rho}(\lambda) = (1 - c)^+ \delta(\lambda) + \frac{\sqrt{(\lambda - a)^+(b - \lambda)^+}}{2\pi\lambda}. \quad (9)$$

In addition to above Wigner's semicircle law and Marchenko-Pastur law, we are also interested in the Single Ring Law developed by Guionnet, Krishnapur and Zeitouni (2011) [46]. It describes the empirical distribution of the eigenvalues of a large generic matrix with prescribed singular values, i.e. an  $N \times N$  matrix of the form  $\mathbf{A} = \mathbf{U}\mathbf{T}\mathbf{V}$ , with  $\mathbf{U}; \mathbf{V}$  some independent Haar-distributed unitary matrices and  $\mathbf{T}$  a deterministic matrix whose singular values are the ones prescribed. More precisely, under some technical hypotheses, as the dimension  $N$  tends to infinity, if the empirical distribution of the singular values of  $\mathbf{A}$  converges to a compactly supported limit measure  $\Theta$  on the real line, then the empirical eigenvalues distribution of  $\mathbf{A}$  converges to a limit measure  $\mu$  on the complex plane which depends only on  $\Theta$ . The limit measure  $\mu$  is rotationally invariant in  $\mathbb{C}$  and its support is the annulus  $S := \{z \in \mathbb{C}; a \leq |z| \leq b\}$  with  $a, b \geq 0$  such that

$$a^{-2} = \int x^{-2} d\Theta(x) \text{ and } b^2 = \int x^2 d\Theta(x). \quad (10)$$

### C. Transforms

The transforms of large random matrices are specially useful to study the limit spectral properties and to tackle the problems of polynomial calculation of random matrices. In this subsection, we will review the useful transforms including Stieltjes transform, R transform and S transform suggested by problems of interest in power grid [49, 56].

We begin with the Stieltjes transform of  $\mathbf{X}$  that is defined as follows.

**Definition II.2.** Let  $\mathbf{X}$  be a random matrix with distribution  $F(\cdot)$ . Its Stieltjes transform is defined as

$$G(z) = \left\{ \frac{1}{N} \text{Tr} \left[ (z\mathbf{I} - \mathbf{X})^{-1} \right] \right\} = \int_{\mathbb{R}} \frac{1}{x - z} dF(x), \quad (11)$$

where  $z \in \mathbb{C}^-$  and  $\mathbb{C}^- = \{z \in \mathbb{C} : \text{Im}(z) < 0\}$  and  $\mathbf{I}$  represents the identity matrix of dimension  $N$ .

An important application of Stieltjes transform is that its close relationship with the limit spectrum density of  $\mathbf{X}$ .

**Theorem II.3.** Let  $\mathbf{X}$  be a  $N \times N$  random hermitian matrix and its Stieltjes transform is  $G(z)$ , the corresponding eigenvalue density  $\rho(x)$  can be expressed as:

$$\rho(x) = -\frac{1}{\pi} \lim_{\text{Im}z \rightarrow 0} \text{Im} \{G(z)\}. \quad (12)$$

It is noted that the signs of the  $\text{Im}(z)$  and  $G(z)$  coincide. This property should be emphasized in the following examples where the sign of the square root should be chosen.

For GUE and LUE matrices, the corresponding Stieltjes transforms are shown in the following examples.

**Example II.4.** Let  $\mathbf{X}$  be an GUE matrix and its limit spectral density is defined in (7), the Stieltjes transform of  $\mathbf{X}$  is

$$G(z) = \frac{1}{2\pi} \int_{-2}^2 \frac{\sqrt{4 - x^2}}{x - z} dx = \frac{1}{2} \left[ z - \sqrt{z^2 - 4} \right].$$

**Example II.5.** Let  $\mathbf{W}$  be an LUE matrix and its limit spectral density is defined in (8) and (9). The corresponding Stieltjes transform can be represented as

$$G(z) = \frac{1}{2\pi} \int_a^b \frac{\rho(x)}{(x - z)} dx = \frac{-\beta - z + 1 \pm \sqrt{z^2 - 2(\beta + 1)z + (\beta - 1)^2}}{2\beta z}$$

and

$$G(z) = \frac{1}{2\pi} \int_a^b \frac{\rho'(x)}{(x - z)} dx = \frac{\beta - z - 1 \pm \sqrt{z^2 - 2(\beta + 1)z + (\beta - 1)^2}}{2z},$$

respectively.

Another two important transforms which we elaborate in the following are R transform and S transform. The key point of these two transforms is that R/S transform enable the characterization of the limiting spectrum of a sum/product of random

matrices from their individual limiting spectra. These properties would turn out to be extremely useful in the following subsection. We start with blue function, that is, the functional inverse of the Stieltjes transform  $G(z)$  which is defined as

$$B(G(z)) = z$$

and then the R transform is simply defined by

$$R(\omega) = B(\omega) - \frac{1}{\omega}$$

Two important prosperities of R transform are shown in the following.

**Additivity law** : let  $R_{\mathbf{A}}(z)$ ,  $R_{\mathbf{B}}(z)$  and  $R_{\mathbf{A}+\mathbf{B}}(z)$  be the R transforms of matrices  $\mathbf{A}$ ,  $\mathbf{B}$  and  $\mathbf{A} + \mathbf{B}$ , respectively. We have

$$R_{\mathbf{A}+\mathbf{B}}(z) = R_{\mathbf{A}}(z) + R_{\mathbf{B}}(z). \quad (13)$$

**Scaling property** : For any  $\alpha > 0$ ,

$$R_{\alpha\mathbf{X}}(z) = \alpha R_{\mathbf{X}}(\alpha z). \quad (14)$$

Additivity law can be easily understood in terms of Feynman diagrams, we refer interested readers to references [49] for details. The above properties of R transform enable us to do the linear calculation of the asymptotic spectrum of random matrices.

Another important transform of engineering significance in RMT is the S transform. S transform is related to the R transform which is defined by

$$S(z) = \frac{1}{R(zS(z))}. \quad (15)$$

An interesting property of S transform is that the S transform of the product of two independent random matrices equals the product of the S transforms:

$$S_{\mathbf{AB}}(z) = S_{\mathbf{A}}(z) S_{\mathbf{B}}(z). \quad (16)$$

Note that (16) is known as multiplication law of S transform. For the sake of brevity, see Section II-E for more details.

#### D. Convergence Rate

In this section, we investigate the spectral asymptotics for GUE and LUE matrices. We are motivated by the practical problems introduced in [49]. Let  $F(x)$  be the empirical spectral distribution function of GUE or LUE matrices and  $G(x)$  be the distribution function of the limit law (semicircle law for GUE matrices and Marchenko-Pastur law for LUE matrices). Here, we study the convergence rate of expected empirical distribution function  $\mathbb{E}F(x)$  to  $G(x)$ . Specially, the bound

$$\Delta = |\mathbb{E}F(x) - G(x)|, \quad (17)$$

is mainly concerned in the following.

The rate of convergence for the expected spectral distribution of GUE matrices has attracted numerous attention due to its increasingly appreciated importance in applied mathematics and statistical physics. Wigner initially looked into the convergence of the spectral distribution of GUE matrices [57]. Bai [58] conjectured that the optimal bound for  $\Delta$  in GUE case should be of order  $n^{-1}$ . Bai and coauthors in [59] proved that  $\Delta = O(N^{-1/3})$ . Gotze and Tikhomirov in [60] improved the result in [59] and proved that  $\Delta = O(N^{-1/2})$ . Bai et al. in [61] also showed that  $\Delta = O(N^{-1/2})$  on the condition that the 8th moment of  $\mathbf{X}$  satisfies  $\sup E|X_{ij}|^8 < \infty$ . Girko in [62] stated as well that  $\Delta = O(N^{-1/2})$  assuming uniform bounded 4th moment of  $\mathbf{X}$ . Recently, Gotze and Tikhomirov proved an optimal bound as follows.

**Theorem II.6.** *There exists a positive constant  $C$  such that, for any  $N \geq 1$ ,*

$$\Delta \leq CN^{-1}. \quad (18)$$

The convergence of the density (denoted by  $g(x)$ ) of standard semicircle law to the expected spectral density  $p(x)$  is proved by Gotze and Tikhomirov in the following Theorem.

**Theorem II.7.** *There exists a positive constant  $\varepsilon$  and  $C$  such that, for any  $x \in [-2 + N^{-\frac{1}{3}}\varepsilon, 2 - N^{-\frac{1}{3}}\varepsilon]$ ,*

$$|p(x) - g(x)| \leq \frac{C}{N(4 - x^2)}. \quad (19)$$



For LUE matrix  $\mathbf{W}$  with spectral distribution function  $F(x)$ , let  $\beta = \frac{N}{M}$  as  $N, M \rightarrow \infty$ , it is well known that  $\mathbb{E}F(x)$  converges to the Marchenko-Pastur law  $H(x)$  with density

$$h(x) = \frac{1}{2\pi\beta x} \sqrt{(x-a)(b-x)}, \quad (20)$$

where  $a = (1 - \sqrt{\beta})^2$ ,  $b = (1 + \sqrt{\beta})^2$ . The bound

$$\Delta = |\mathbb{E}F(x) - H(x)|, \quad (21)$$

for the convergence rate is shown in the following theorems.

**Theorem II.8.** *For  $\beta = \frac{N}{M}$ , there exist some positive constant  $\beta_1$  and  $\beta_2$  such that  $0 < \beta_1 \leq \beta \leq \beta_2 < 1$ , for all  $N \geq 1$ . Then there exists a positive constant  $C$  depending on  $\beta_1$  and  $\beta_2$  and for any  $N \geq 1$*

$$\Delta \leq CN^{-1}. \quad (22)$$

Considering the case  $\beta < 1$ , a similar result is shown in Theorem II.9.

**Theorem II.9.** *For  $\beta = \frac{N}{M}$ , there exists some positive constant  $\beta_1$  and  $\beta_2$  such that  $0 < \beta_1 \leq \beta \leq \beta_2 < 1$ , for all  $N \geq 1$ . Then there exists a positive constant  $C$  and  $\varepsilon$  depending on  $\beta_1$  and  $\beta_2$  and for any  $N \geq 1$  and  $x \in [a + N^{-\frac{2}{3}}\varepsilon, b - N^{-\frac{2}{3}}\varepsilon]$*

$$|p(x) - h(x)| \leq \frac{C}{N(x-a)(b-x)}. \quad (23)$$

Interested readers are referred to [63] for technical details and Section III-C for applications in smart grid.

### E. Free Probability

Free probability theory, initiated in 1983 by Voiculescu in [64], together with the results published in [65] regarding asymptotic freeness of random matrices, has established a new branch of theories and tools in random matrix theory. Here, we provide some of the basic principles and then examples to enhance the understanding and application of the free probability theory.

Let  $x_1, \dots, x_n$  be selfadjoint elements which are freely independent. Consider a selfadjoint polynomial  $p$  in  $n$  non-commuting variables and let  $P$  be the element  $P = p(x_1, \dots, x_n)$ . Now we introduce the method [66] [67] to obtain the distribution of  $P$  out of the distributions of  $x_1, \dots, x_n$ .

Let  $\mathcal{A}$  be a unital algebra and  $\mathcal{B} \subset \mathcal{A}$  be a subalgebra containing the unit. A linear map

$$E : \mathcal{A} \rightarrow \mathcal{B}$$

is a conditional expectation if

$$E[b] = b \quad \text{for all } b \in \mathcal{B}$$

and

$$E[b_1 a b_2] = b_1 E[a] b_2 \quad \text{for all } a \in \mathcal{A} \text{ for all } b_1, b_2 \in \mathcal{B}$$

An operator-valued probability space consists of  $\mathcal{B} \subset \mathcal{A}$  and a conditional expectation  $E : \mathcal{A} \rightarrow \mathcal{B}$ . Then, random variables  $x_i \in \mathcal{A} (i \in I)$  are free with respect to  $E$  (or free with amalgamation over  $\mathcal{B}$ ) if  $E[a_1 \dots a_n] = 0$  whenever  $a_i \in \mathcal{B} < x_{j(i)} >$  are polynomials in some  $x_{j(i)}$  with coefficients from  $\mathcal{B}$  and  $E[a_i] = 0$  for all  $i$  and  $j(1) \neq j(2) \neq \dots \neq j(n)$ . For a random variable  $x \in \mathcal{A}$ , we denote the operator-valued Cauchy transform:

$$G(b) := E[(b-x)^{-1}] (b \in \mathcal{B})$$

whenever  $(b-x)$  is invertible in  $\mathcal{B}$ . In order to have some nice analytic behaviour, we assume that both  $\mathcal{A}$  and  $\mathcal{B}$  are  $C^*$ -algebras in the following;  $\mathcal{B}$  will usually be of the form  $\mathcal{B} = M_N(\mathbb{C})$ , the  $N \times N$ -matrices. In such a setting and for  $x = x^*$ , this  $G$  is well-defined and a nice analytic map on the operator-valued upper halfplane:

$$\mathbb{H}^+(B) := \{b \in B | (b - b^*)/(2i) > 0\}$$

and it allows to give a nice description for the sum of two free selfadjoint elements. In the following we will use the notation

$$h(b) := \frac{1}{G(b)} - b$$

**Theorem II.10.** ([66]) *Let  $x$  and  $y$  be selfadjoint operator-valued random variables free over  $\mathcal{B}$ . Then there exists a Frechet analytic map  $\omega : \mathbb{H}^+(\mathcal{B}) \rightarrow \mathbb{H}^+(\mathcal{B})$  so that*

- $\Im \omega_j(b) \geq \Im b$  for all  $b \in \mathbb{H}^+(\mathcal{B})$ ,  $j \in \{1, 2\}$
- $G_x(\omega_1(b)) = G_y(\omega_2(b)) = G_{x+y}(b)$

Moreover, if  $b \in \mathbb{H}^+(\mathcal{B})$ , then  $\omega_1(b)$  is the unique fixed point of the map.  $f_b : \mathbb{H}^+(\mathcal{B}) \rightarrow \mathbb{H}^+(\mathcal{B})$ ,  $f_b(\omega) = h_y(h_x(\omega) + b) + b$ , and  $\omega_1(b) = \lim_{n \rightarrow \infty} f_b^{on}(\omega)$  for any  $\omega \in \mathbb{H}^+(\mathcal{B})$ , where  $f_b^{on}$  means the  $n$ -fold composition of  $f_b$  with itself. Same statements hold for  $\omega_2(b)$ , replaced by  $\omega \rightarrow h_x(h_y(\omega) + b) + b$ .

Let  $\mathcal{A}$  be a complex and unital  $C^*$ -algebra and let selfadjoint elements  $x_1, \dots, x_n \in \mathcal{A}$ .  $\mathcal{A}$  is given. Then, for any non-commutative polynomial  $p \in \mathbb{C} \langle \mathbf{X}_1, \dots, \mathbf{X}_n \rangle$ , we get an operator  $P = p(x_1, \dots, x_n) \in \mathcal{A}$  by evaluating  $p$  at  $(x_1, \dots, x_n)$ . In this situation, knowing a linearization trick [68] means to have a procedure that leads finally to an operator

$$L_p = b_0 \otimes 1 + b_1 \otimes x_1 + \dots + b_n \otimes x_n \in M_N(\mathbb{C}) \otimes \mathcal{A}$$

for some matrices  $b_0, \dots, b_n \in M_N(\mathbb{C})$  of dimension  $N$ , such that  $z - P$  is invertible in  $\mathcal{A}$  if and only if  $\Lambda(z) - L_p$  is invertible in  $M_N(\mathbb{C}) \otimes \mathcal{A}$ . Hereby, we put

$$\Lambda(z) = \begin{bmatrix} z & 0 & \dots & 0 \\ 0 & 0 & \dots & 0 \\ \vdots & \vdots & \ddots & \vdots \\ 0 & 0 & \dots & 0 \end{bmatrix} \quad \text{for all } z \in \mathbb{C}.$$

Let  $p \in \mathbb{C} \langle \mathbf{X}_1, \dots, \mathbf{X}_n \rangle$  be given. A matrix

$$L_p := \begin{bmatrix} 0 & u \\ v & \mathbf{Q} \end{bmatrix} \in M_N(\mathbb{C}) \otimes \mathbb{C} \langle \mathbf{X}_1, \dots, \mathbf{X}_n \rangle$$

where

- $N \in \mathbb{N}$  is an integer,
- $\mathbf{Q} \in M_{N-1}(\mathbb{C}) \otimes \mathbb{C} \langle \mathbf{X}_1, \dots, \mathbf{X}_n \rangle$  is invertible,
- and  $u$  is a row vector and  $v$  is a column vector, both of size  $N - 1$  with entries in  $\mathbb{C} \langle \mathbf{X}_1, \dots, \mathbf{X}_n \rangle$ ,

is called a linearization of  $p$ , if the following conditions are satisfied:

- 1) There are matrices  $b_0, \dots, b_n \in M_N(\mathbb{C})$ , such that

$L_p = b_0 \otimes 1 + b_1 \otimes \mathbf{X}_1 + \dots + b_n \otimes \mathbf{X}_n$  i.e. the polynomial entries in  $\mathbf{Q}$ ,  $u$  and  $v$  all have degree  $\leq 1$ .

- 2) It holds true that  $p = -u\mathbf{Q}^{-1}v$ .

To introduce the following corollary, which will enable us to shift  $\Lambda_\varepsilon(z)$  for  $z \in \mathbb{C}^+$  to a point

$$\Lambda_\varepsilon(z) := \begin{bmatrix} z & & & \\ & i\varepsilon & & \\ & & \ddots & \\ & & & i\varepsilon \end{bmatrix}$$

lying inside the domain  $\mathbb{H}^+(M_N(\mathbb{C}))$  in order to get access to all analytic tools that are available there.

**Corollary II.11.** Let  $(\mathcal{A}, \phi)$  be a  $C^*$ -probability space and let elements  $x_1, \dots, x_n \in \mathcal{A}$  be given. For any selfadjoint  $p \in \mathbb{C} \langle \mathbf{X}_1, \dots, \mathbf{X}_n \rangle$  that has a selfadjoint linearization

$$L_p = b_0 \otimes 1 + b_1 \otimes \mathbf{X}_1 + \dots + b_n \otimes \mathbf{X}_n \in M_N(\mathbb{C}) \otimes \mathbb{C} \langle \mathbf{X}_1, \dots, \mathbf{X}_n \rangle$$

with matrices  $b_0, \dots, b_n \in M_N(\mathbb{C})_{sa}$ , we put  $P = p(x_1, \dots, x_n)$  and

$$L_P = b_0 \otimes 1 + b_1 \otimes x_1 + \dots + b_n \otimes x_n \in M_N(\mathbb{C}) \otimes \mathcal{A}$$

Then, for each  $z \in \mathbb{C}^+$  and all sufficiently small  $\varepsilon > 0$ , the operators  $z - P \in \mathcal{A}$  and  $\Lambda_\varepsilon(z) - L_P \in M_N(\mathbb{C}) \otimes \mathcal{A}$  are both invertible and we have

$$\lim_{\varepsilon \rightarrow 0} \left[ \mathbb{E}((\Lambda_\varepsilon(z) - L_P)^{-1}) \right]_{1,1} = G_P(z)$$

Hereby,

$$\mathbb{E} M_N(\mathbb{C}) \otimes \mathcal{A} \rightarrow M_N(\mathbb{C})$$

denotes the conditional expectation given by  $\mathbb{E} = id_{M_N(\mathbb{C})} \otimes \phi$ .

Let  $(\mathcal{A}, \phi)$  be a non-commutative  $C^*$ -probability space,  $x_1, \dots, x_n \in \mathcal{A}$  selfadjoint elements which are freely independent, and  $p \in \mathbb{C} \langle \mathbf{X}_1, \dots, \mathbf{X}_n \rangle$  a selfadjoint polynomial in  $n$  non-commuting variables  $\mathbf{X}_1, \dots, \mathbf{X}_N$ . We put  $P = p(x_1, \dots, x_n)$ . The following procedure leads to the distribution of  $P$ .

step 1  $p$  has a selfadjoint linearization

$$L_p = b_0 \otimes 1 + b_1 \otimes \mathbf{X}_1 + \dots + b_n \otimes \mathbf{X}_n$$

with matrices  $b_0, \dots, b_n \in M_N \mathbb{C}_{\text{sa}}$ . We put

$$L_P = b_0 \otimes 1 + b_1 \otimes x_1 + \dots b_n \otimes x_n \in M_N(\mathbb{C}) \otimes \mathcal{A}.$$

step 2 The operators  $b_0 \otimes 1, b_1 \otimes x_1, \dots, b_n \otimes x_n$  are freely independent elements in the operator-valued  $C^*$ -probability space  $(M_N(\mathbb{C}) \otimes \mathcal{A}, \mathbb{E})$ , where  $\mathbb{E} := M_N(\mathbb{C}) \otimes \mathcal{A} \rightarrow M_N(\mathbb{C})$  denotes the conditional expectation given by  $\mathbb{E} = \text{id}_{M_N(\mathbb{C})} \otimes \phi$ . Furthermore, for  $j = 1, \dots, n$ , the  $M_N(\mathbb{C})$ -valued Cauchy transform  $G_{b_j \otimes x_j}(b)$  is completely determined by the scalar-valued Cauchy transforms  $G_{x_j}$  via

$$G_{b_j \otimes x_j}(b) = \lim_{\varepsilon \rightarrow 0} -\frac{1}{\pi} \int_{\mathbb{R}} (b - tb_j)^{-1} \Im(G_{x_j}(t + i\varepsilon)) dt$$

for all  $b \in \mathbb{H}^+(M_N(\mathbb{C}))$ .

step 3 Due to Step 3, we can calculate the Cauchy transform of

$$L_P - b_0 \otimes 1 = b_1 \otimes \mathbf{X}_1 + \dots b_n \otimes \mathbf{X}_n$$

by using the fixed point iteration for the operator-valued free additive convolution. The Cauchy transform of  $L_P$  is then given by

$$G_{L_P}(b) = G_{L_P - b_0 \otimes 1}(b - b_0) \quad \text{for all } b \in \mathbb{H}^+(M_N(\mathbb{C}))$$

step 4 Corollary tells us that the scalar-valued Cauchy transform  $G_P(z)$  of  $P$  is determined by

$$G_P(z) = \lim_{\varepsilon \rightarrow 0} [G_{L_P}(\Lambda_\varepsilon(z))]_{1,1} \quad \text{for all } z \in \mathbb{C}^+$$

Finally, we obtain the desired distribution of  $P$  by applying the Stieltjes inversion formula.

**Example II.12.** We consider the non-commutative polynomial  $p \in \mathbb{C} \langle \mathbf{X}_1, \mathbf{X}_2 \rangle$  given by  $p(\mathbf{X}_1, \mathbf{X}_2) = \mathbf{X}_1 \mathbf{X}_2 + \mathbf{X}_2 \mathbf{X}_1$ . It is easy to check that

$$L_p = \begin{bmatrix} 0 & \mathbf{X}_1 & \mathbf{X}_2 \\ \mathbf{X}_1 & 0 & -1 \\ \mathbf{X}_2 & -1 & 0 \end{bmatrix}$$

is a selfadjoint linearization of  $p$ . Now, let  $X_1, X_2$  be free semicircular or Poisson elements in a non-commutative  $C^*$ -probability space  $(\mathcal{A}, \phi)$ . Based on the algorithm of Theorem above, we can calculate the distribution of the anticommutator  $p(\mathbf{X}_1, \mathbf{X}_2) = \mathbf{X}_1 \mathbf{X}_2 + \mathbf{X}_2 \mathbf{X}_1$ .

**Example II.13.** In the same way, we can deal with the following variation of the anticommutator:  $p(\mathbf{X}_1, \mathbf{X}_2) = \mathbf{X}_1 \mathbf{X}_2 + \mathbf{X}_2 \mathbf{X}_1 + \mathbf{X}_1^2$ . It is easy to check that

$$L_p = \begin{bmatrix} 0 & \mathbf{X}_1 & \frac{1}{2} \mathbf{X}_1 + \mathbf{X}_2 \\ \mathbf{X}_1 & 0 & -1 \\ \frac{1}{2} \mathbf{X}_1 + \mathbf{X}_2 & -1 & 0 \end{bmatrix}$$

is a selfadjoint linearization of  $p$ .

Then, let  $\mathbf{X}_1, \mathbf{X}_2$  be free semicircular or Poisson elements in a non-commutative  $C^*$ -probability space  $(\mathcal{A}, \phi)$ . Based on the algorithm above, we can calculate the distribution of the polynomial  $p(\mathbf{X}_1, \mathbf{X}_2) = \mathbf{X}_1 \mathbf{X}_2 + \mathbf{X}_2 \mathbf{X}_1 + \mathbf{X}_1^2$ .

For readers's convenience, we also provide some simulations of the free polynomials of random matrices in the following.

### III. APPLICATIONS TO SMART GRIDS

In this section, we elaborate some of the more representative problems described in Section I that capture various features of interest in smart grid and we show how random matrix results have been used to tackle the problems that arise in the large power grid with wide deployment of PMU equipments. Besides, we also conclude some state-of-art data driven methods for comparison.

#### A. Hypothesis Tests in Smart Grids

Considering the data model introduced in Section II-A, the problem of testing hypotheses on means of populations and covariance matrices is addressed. We stated by a review of traditional multivariate procedures for these tests. Then we develop adjustments of these procedures to handle with high-dimensional data in smart grid.

As depicted in the Section II-A, a large random matrix flow  $\{\mathbf{Z}_1, \mathbf{Z}_2, \dots, \mathbf{Z}_q\}$  is adopted to represent the massive streaming PMU data in one sample period. Instead of analyzing the raw individual window-truncated PMU data  $\mathbf{Z}_g$  [38, 39] or the

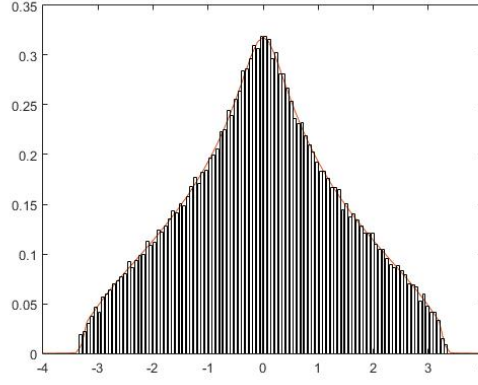


Fig. 6. Comparison of the distribution of  $p(\mathbf{X}_1, \mathbf{X}_2) = \mathbf{X}_1\mathbf{X}_2 + \mathbf{X}_2\mathbf{X}_1$  according to our algorithm, with the histogram of eigenvalues for  $p(\mathbf{X}_1^{(n)}, \mathbf{X}_2^{(n)})$  according to our algorithm, with the histogram of eigenvalues for  $p(\mathbf{X}_1^{(n)}, \mathbf{X}_2^{(n)})$ , for  $n = 1000$ .  $\mathbf{X}_1, \mathbf{X}_2$  are free semicircular elements and  $\mathbf{X}_1^{(n)}, \mathbf{X}_2^{(n)}$  are independent standard Gaussian random matrices.

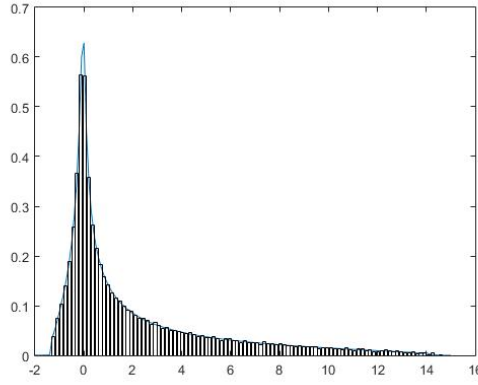


Fig. 7. Comparison of the distribution of  $p(\mathbf{X}_1, \mathbf{X}_2) = \mathbf{X}_1\mathbf{X}_2 + \mathbf{X}_2\mathbf{X}_1$  according to our algorithm, with the histogram of eigenvalues for  $p(\mathbf{X}_1^{(n)}, \mathbf{X}_2^{(n)})$ , for  $n = 1000$ .  $\mathbf{X}_1, \mathbf{X}_2$  are free poisson elements and  $\mathbf{X}_1^{(n)}, \mathbf{X}_2^{(n)}$  are Wishart random matrices.

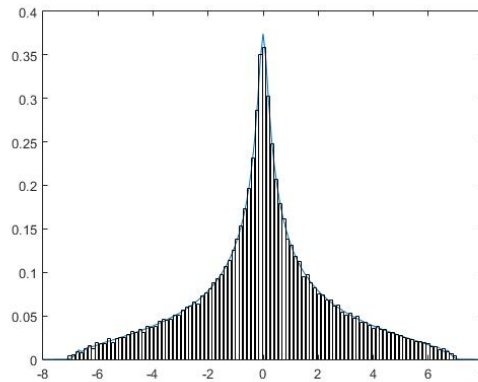


Fig. 8. Comparison of the distribution of  $p(\mathbf{X}_1, \mathbf{X}_2) = \mathbf{X}_1\mathbf{X}_2 + \mathbf{X}_2\mathbf{X}_1$  according to our algorithm, with the histogram of eigenvalues for  $p(\mathbf{X}_1^{(n)}, \mathbf{X}_2^{(n)})$ , for  $n = 1000$ .  $\mathbf{X}_1$  is of free semicircular elements and  $\mathbf{X}_2$  free Poisson ones.  $\mathbf{X}_1^{(n)}$  is an independent standard Gaussian random matrix and  $\mathbf{X}_2^{(n)}$  is a Wishart matrix.

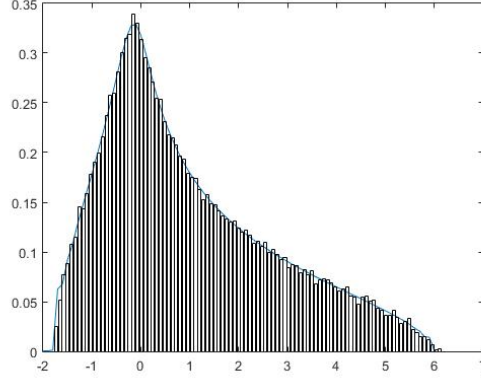


Fig. 9. Comparison of the distribution of  $p(\mathbf{X}_1, \mathbf{X}_2) = \mathbf{X}_1\mathbf{X}_2 + \mathbf{X}_2\mathbf{X}_1 + \mathbf{X}_1^2$  according to our algorithm, with the histogram of eigenvalues for  $p(\mathbf{X}_1^{(n)}, \mathbf{X}_2^{(n)})$ , for  $n = 1000$ .  $\mathbf{X}_1, \mathbf{X}_2$  are of free poisson elements and  $\mathbf{X}_1^{(n)}, \mathbf{X}_2^{(n)}$  are Wishart random matrices.

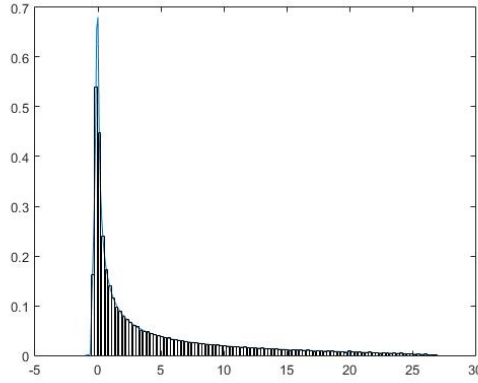


Fig. 10. Comparison of the distribution of  $p(\mathbf{X}_1, \mathbf{X}_2) = \mathbf{X}_1\mathbf{X}_2 + \mathbf{X}_2\mathbf{X}_1 + \mathbf{X}_1^2$  according to our algorithm, with the histogram of eigenvalues for  $p(\mathbf{X}_1^{(n)}, \mathbf{X}_2^{(n)})$ , for  $n = 1000$ .  $\mathbf{X}_1, \mathbf{X}_2$  are of free poisson elements and  $\mathbf{X}_1^{(n)}, \mathbf{X}_2^{(n)}$  are Wishart random matrices.

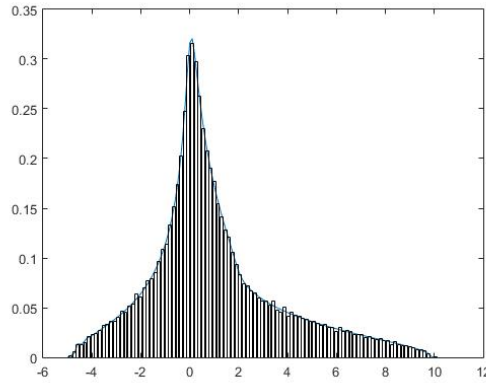


Fig. 11. Comparison of the distribution of  $p(\mathbf{X}_1, \mathbf{X}_2) = \mathbf{X}_1\mathbf{X}_2 + \mathbf{X}_2\mathbf{X}_1 + \mathbf{X}_1^2$  according to our algorithm, with the histogram of eigenvalues for  $p(\mathbf{X}_1^{(n)}, \mathbf{X}_2^{(n)})$ , for  $n = 1000$ .  $\mathbf{X}_1$  are of free semicircular elements and  $\mathbf{X}_2$  free Poisson ones.  $\mathbf{X}_1^{(n)}$  is an independent standard Gaussian random matrix and  $\mathbf{X}_2^{(n)}$  is a Wishart matrix.

statistic of  $\mathbf{Z}_g$  [52, 53], a comprehensive analysis of the statistic of  $\{\mathbf{Z}_1, \mathbf{Z}_2, \dots, \mathbf{Z}_q\}$  is conducted in the following. More specially, denote  $\Sigma_i$  as the covariance matrix of  $i$ th collected PMU measurements, we want to test the hypothesis:

$$\begin{aligned} H_0 : \Sigma_1 = \Sigma_2 = \dots = \Sigma_q \\ H_1 : \exists j, k \text{ s.t. } \Sigma_j \neq \Sigma_k \end{aligned} \quad (24)$$

It is worthy noting that the hypothesis (24) is a famous testing hypothesis in multivariate statistical analysis which aims to study samples share or approximately share some same distribution and consider using a set of samples (data streams denoted in equation (4) in this paper), one from each population, to test the hypothesis that the covariance matrices of these populations are equal.

### B. Data Driven Methods for State Evaluation

The LR test [69] and CLR test [70] as introduced in the Section III-A are most commonly test statistics for the hypothesis in (24). These tests can be understood by replacing the population covariance matrix  $\Sigma_g$  by its sample covariance matrix  $\mathbf{Y}_g$ . While direct substitution of  $\Sigma_g$  by  $\mathbf{Y}_g$  brings invariance and good testing properties as shown in [69] for normally distributed data. The test statistic  $V_2$  may not work for high-dimensional data as demonstrated in [71, 72]. Besides, the estimator  $V_3$  has unnecessary terms which slow down the convergence considerably when dimension of PMU data is high [72, 73]. In such situations, to overcome the drawbacks, trace criterion [72] is more suitable to the test problem. Specially, instead of estimating the population covariance matrix directly, a well defined distance measure exploiting the difference among data flow  $\{\mathbf{Z}_1, \mathbf{Z}_2, \dots, \mathbf{Z}_q\}$  is conducted, that is, the trace-based distance measure between  $\Sigma_s$  and  $\Sigma_t$  is

$$\text{tr} \left\{ (\Sigma_s - \Sigma_t)^2 \right\} = \text{tr} (\Sigma_s^2) + \text{tr} (\Sigma_t^2) - 2\text{tr} (\Sigma_s \Sigma_t), \quad (25)$$

where  $\text{tr}(\cdot)$  is the trace operator. Instead of estimating  $\text{tr}(\Sigma_s^2)$ ,  $\text{tr}(\Sigma_t^2)$  and  $\text{tr}(\Sigma_s \Sigma_t)$  by sample covariance matrix based estimators, we adopt the merits of the U-statistics [74]. Specially, for  $l = \{s, t\} \in \Omega = \{1 \leq s, t \leq q, s \neq t\}$ ,

$$\begin{aligned} A_l &= \frac{1}{n_g(n_g - 1)} \sum_{i \neq j} \left( \mathbf{z}'_{li} \mathbf{z}_{lj} \right)^2 \\ &- \frac{2}{n_g(n_g - 1)(n_g - 2)} \sum_{i, j, k}^* \mathbf{z}'_{li} \mathbf{z}_{lj} \mathbf{z}'_{lk} \mathbf{z}_{lk} \\ &+ \frac{1}{n_g(n_g - 1)(n_g - 2)(n_g - 3)} \sum_{i, j, k, h}^* \mathbf{z}'_{li} \mathbf{z}_{lj} \mathbf{z}'_{lk} \mathbf{z}_{lh} \end{aligned} \quad (26)$$

is proposed to estimate  $\text{tr}(\Sigma_l^2)$ . It is noted that  $\sum^*$  represents summation over mutually distinct indices. For example,  $\sum_{i, j, k}^*$  says summation over the set  $\{(i, j, k) : i \neq j, j \neq k, k \neq i\}$ . Similarly, the estimator for  $\text{tr}(\Sigma_s \Sigma_t)$  can be expressed as

$$\begin{aligned} C_{st} &= \frac{1}{n_g^2} \sum_i \sum_j \left( \mathbf{z}'_{si} \mathbf{z}_{tj} \right)^2 \\ &- \frac{1}{(n_g - 1)n_g^2} \sum_{i, h}^* \sum_j \mathbf{z}'_{si} \mathbf{z}_{tj} \mathbf{z}'_{th} \mathbf{z}_{sj} \\ &- \frac{1}{(n_g - 1)n_g^2} \sum_{i, l}^* \sum_j \mathbf{z}'_{ti} \mathbf{z}_{sj} \mathbf{z}'_{sl} \mathbf{z}_{th} \\ &+ \frac{1}{(n_g - 1)^2 n_g^2} \sum_{i, h}^* \sum_{j, k}^* \mathbf{z}'_{si} \mathbf{z}_{tj} \mathbf{z}'_{sk} \mathbf{z}_{th}. \end{aligned} \quad (27)$$

The test statistic which measures the distance between  $\Sigma_s$  and  $\Sigma_t$  is

$$V_{st} = A_s + A_t - C_{st}. \quad (28)$$

Then the proposed test statistic can be expressed as:

$$V_1 = \frac{1}{q(q-1)} \sum_{\{s, t\} \in \Omega} T_{st}. \quad (29)$$

As  $p, n_g \rightarrow \infty$ , the asymptotic normality [73] of the test statistic (28) is presented in the following:

**Theorem III.1.** Let  $\sigma_{st}^2 = \frac{1}{n_g} (A_s + A_t)$ . Assuming the following conditions:

- 1) For any  $k$  and  $l \in \{s, t\}$ ,  $\text{tr}(\Sigma_k \Sigma_l) \rightarrow \infty$  and

$$\text{tr} \{ (\Sigma_i \Sigma_j) (\Sigma_k \Sigma_l) \} = O \{ \text{tr}(\Sigma_i \Sigma_j) \text{tr}(\Sigma_k \Sigma_l) \}.$$

2) For  $i = 1, 2, \dots, n_g$ ,  $\mathbf{z}^{(i)}$  are independent and identically distributed  $p$ -dimensional vectors with finite 8th moment. Under above conditions,

$$L = \frac{V_{st}}{\sigma_{st}} \xrightarrow{d} \mathcal{N}(0, 1)$$

**Corollary III.2.** For any  $q \geq 2$ , as  $p, n_g \rightarrow \infty$ , the proposed test statistic  $V_1$  satisfies

$$V_1 \xrightarrow{d} \mathcal{N}(\mu, \sigma^2), \quad (30)$$

where  $\mu \approx 0, \sigma^2 = \sum^* \sigma_{st}^2$ .

Let  $R = \frac{V_1}{\sigma_{V_1}}$ , the false alarm probability (FAP) for the proposed test statistic can be represented as

$$\begin{aligned} P_{FAP} &= P(R > \alpha | H_0) \\ &= \int_R^\infty \frac{1}{\sqrt{2\pi}} \exp\left(-\frac{t^2}{2}\right) dt \\ &= Q(R), \end{aligned} \quad (31)$$

where  $Q(x) = \int_x^\infty 1/\sqrt{2\pi} \exp(-t^2/2) dt$ . For a desired FAP  $\tau$ , the associated threshold should be chosen such that

$$\alpha = Q^{-1}(\tau).$$

Otherwise, the detection rate (DR) can be denoted as

$$P_{DR} = P(R \geq Q(\alpha) | H_1). \quad (32)$$

It is noted that the computation complexity of proposed test statistic in (30) is  $O(\varepsilon n_g^4)$  which limits its practical application. Here, we proposed a effective approach to reducing complexity of the proposed test statistic from  $O(\varepsilon n_g^4)$  to  $O(\eta n_g^2)$  by principal component calculation and redundant computation elimination. For simplicity, we briefly explained the technical details in our recent work which is available at <https://arxiv.org/abs/1609.03301>.

In this section, we evaluate the efficacy of the proposed test statistic for power system stability. For the experiments shown in the following, the real power flow data were of a chain-reaction fault happened in the China power grids in 2013. The PMU number, the sample rate and the total sample time are  $p = 34$ ,  $K = 50\text{Hz}$  and  $284\text{s}$ , respectively. The chain-reaction fault happened from  $t = 65.4\text{s}$  to  $t = 73.3\text{s}$ . Let  $q = 5, n_g = 50$ . Fig.12 shows that the mean and variance of  $\lambda$  agree well with theoretical ones. Based on the results in Fig.12 and event indicators (29), the occurrence time and the actual duration of the event can be identified as  $t_0 = 65\text{s}$  and  $t_{dur} \approx 8\text{s}$ , respectively. The location of the most sensitive bus can also be identified using the data analysis above. The result shown in Fig.13 illustrates that 17th and 18th PMU are the most sensitive PMUs which are in accordance with the actual accident situation.

### C. Situation Awareness based on Linear Eigenvalue Statistics

Situation awareness (SA) is of great significance in power system operation, and a reconsideration of SA is essential for future grids [24]. These future grids are always huge in size and complex in topology. Operating under a novel regulation, their management mode is much different from previous one.

All these driving forces demand a new prominence to the term situation awareness (SA). The SA is essential for power grid security; inadequate SA is identified as one of the root causes for the largest blackout in history—the 14 August 2003 Blackout in the United States and Canada [75].

In [76], SA is defined as the perception of the elements in an environment, the comprehension of their meaning, and the projection of their status in the near future. This chapter is aimed at the use of model-free and data-driven methodology for the comprehension of the power grid.

The massive data compose the profile of the actual grid—present state; SA aims to translate the present state into perceived state for decision-making [77].

The proposed methodology consists of three essential procedures as illustrated in Fig. 14(b): 1) big data model—to model the system using experimental data for the RMM; 2) big data analysis—to conduct high-dimensional analyses for the indicator system as the statistical solutions; 3) engineering interpretation—to visualize and interpret the statistical results to human beings for decision-making.

Power grids operate in a balance situation obeying

$$\begin{cases} \Delta P_i = P_{is} - P_i(\mathbf{v}, \boldsymbol{\theta}) \\ \Delta Q_i = Q_{is} - Q_i(\mathbf{v}, \boldsymbol{\theta}) \end{cases}, \quad (33)$$

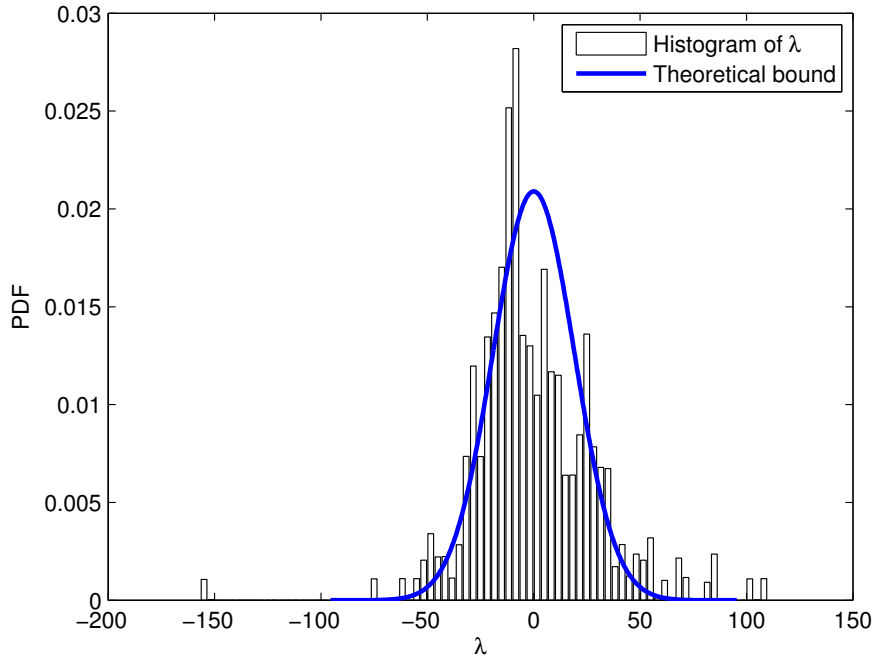


Fig. 12. Parameter learning of the IEEE 118-bus system.

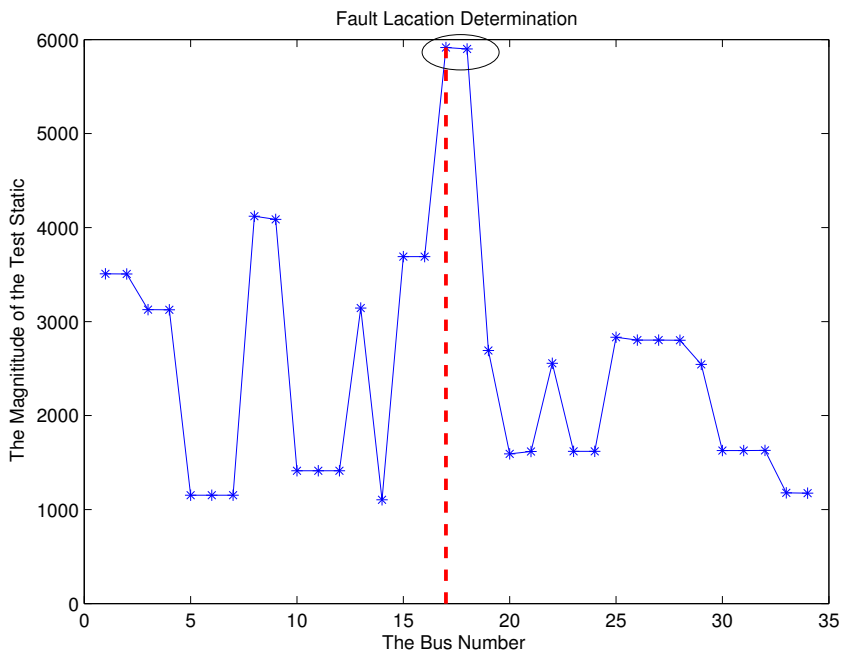


Fig. 13. Data analysis of the realistic 34-PMU power flow around events occurrence.



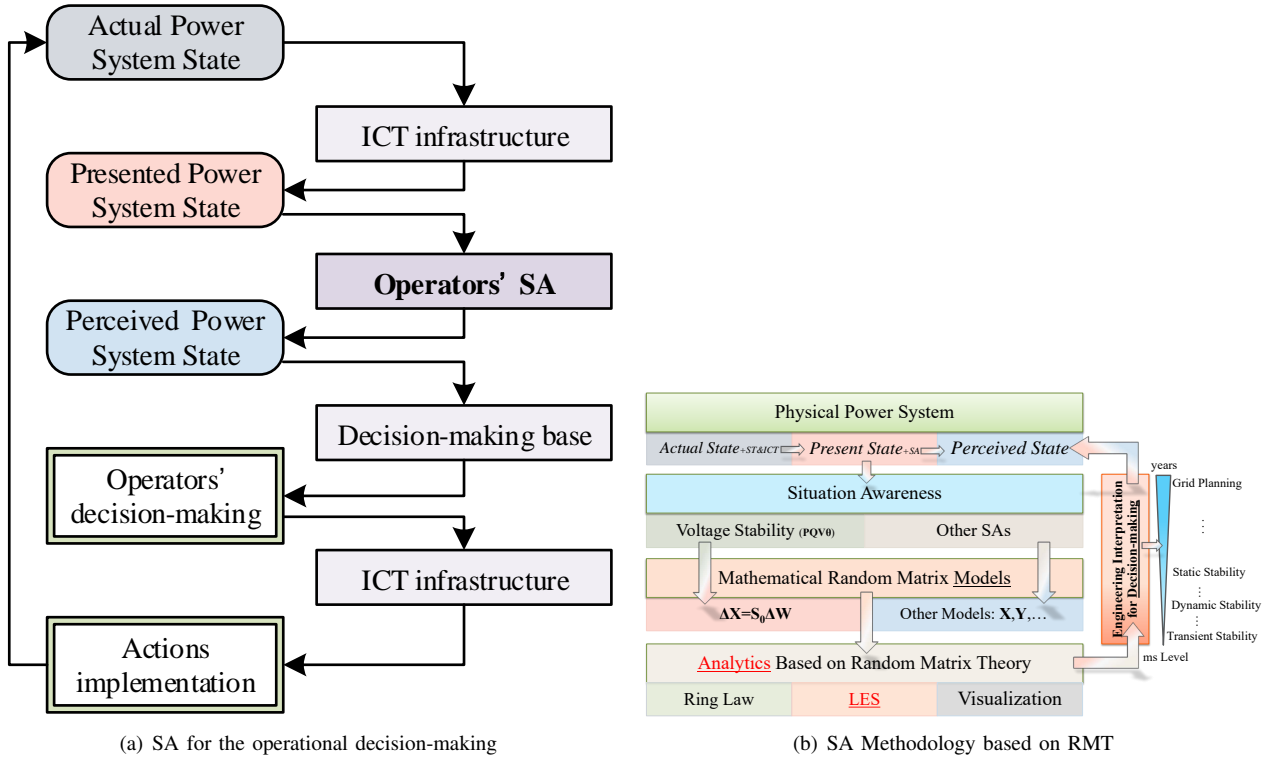


Fig. 14. SA and its methodology

where  $P_{is}$  and  $Q_{is}$  are the power injections on node  $i$ , while  $P_i(\mathbf{v}, \boldsymbol{\theta})$  and  $Q_i(\mathbf{v}, \boldsymbol{\theta})$  are the injections of the network satisfying

$$\begin{cases} P_i = V_i \sum_{j=1}^n V_j (G_{ij} \cos \theta_{ij} + B_{ij} \sin \theta_{ij}) \\ Q_i = V_i \sum_{j=1}^n V_j (G_{ij} \sin \theta_{ij} - B_{ij} \cos \theta_{ij}) \end{cases} \quad (34)$$

For simplicity, combining (33) and (34), we obtain

$$\mathbf{W}_0 = f(\mathbf{X}_0, \mathbf{Y}_0), \quad (35)$$

where  $\mathbf{W}_0$  is the vector of power injections on nodes depending on  $P_{is}$ ,  $Q_{is}$ .  $\mathbf{X}_0$  is the system status variables depending on  $V_i$ ,  $\theta_i$ , while  $\mathbf{Y}_0$  is the network topology parameters depending on  $B_{ij}$ ,  $G_{ij}$ .

For a system state with certain fluctuations—thus randomness in datasets, we formulate the system as

$$\mathbf{W}_0 + \Delta \mathbf{W} = f(\mathbf{X}_0 + \Delta \mathbf{X}, \mathbf{Y}_0 + \Delta \mathbf{Y}). \quad (36)$$

With a Taylor expansion, (36) is rewritten as

$$\begin{aligned} \mathbf{W}_0 + \Delta \mathbf{W} = & f(\mathbf{X}_0, \mathbf{Y}_0) + f'_{\mathbf{X}}(\mathbf{X}_0, \mathbf{Y}_0) \Delta \mathbf{X} + f'_{\mathbf{Y}}(\mathbf{X}_0, \mathbf{Y}_0) \Delta \mathbf{Y} \\ & + \frac{1}{2} f''_{\mathbf{X}\mathbf{X}}(\mathbf{X}_0, \mathbf{Y}_0) (\Delta \mathbf{X})^2 + \frac{1}{2} f''_{\mathbf{Y}\mathbf{Y}}(\mathbf{X}_0, \mathbf{Y}_0) (\Delta \mathbf{Y})^2 \\ & + f''_{\mathbf{X}\mathbf{Y}}(\mathbf{X}_0, \mathbf{Y}_0) \Delta \mathbf{X} \Delta \mathbf{Y} + \dots \end{aligned} \quad (37)$$

Equ. (34) shows that  $\mathbf{W}_0$  is linear with  $\mathbf{Y}_0$ ; it means that  $f''_{\mathbf{Y}\mathbf{Y}}(\mathbf{X}, \mathbf{Y}) = 0$ . On the other hand, the value of system status variables  $\mathbf{X}$  are relatively stable and we can ignore the second-order term  $(\Delta \mathbf{X})^2$  and higher-order terms. In this way, we turn (37) into

$$\begin{aligned} \Delta \mathbf{W} = & f'_{\mathbf{X}}(\mathbf{X}_0, \mathbf{Y}_0) \Delta \mathbf{X} + f'_{\mathbf{Y}}(\mathbf{X}_0, \mathbf{Y}_0) \Delta \mathbf{Y} \\ & + f''_{\mathbf{X}\mathbf{Y}}(\mathbf{X}_0, \mathbf{Y}_0) \Delta \mathbf{X} \Delta \mathbf{Y}. \end{aligned} \quad (38)$$

Suppose the network topology is unchanged, i.e.,  $\Delta \mathbf{Y} = 0$ . From (38), we deduce that

$$\Delta \mathbf{X} = (f'_{\mathbf{X}}(\mathbf{X}_0, \mathbf{Y}_0))^{-1} (\Delta \mathbf{W}) = \mathbf{S}_0 \Delta \mathbf{W}. \quad (39)$$

On the other hand, suppose the power demands is unchanged, i.e.,  $\Delta \mathbf{W} = 0$ . From (38), we obtain that

$$\Delta \mathbf{X} = \mathbf{S}_0 \Delta \mathbf{W}_y, \quad (40)$$

where  $\mathbf{W}_y = [\mathbf{I} + f''_{\mathbf{X}\mathbf{Y}}(\mathbf{X}_0, \mathbf{Y}_0) \Delta \mathbf{Y} \mathbf{S}_0]^{-1} [f'_{\mathbf{Y}}(\mathbf{X}_0, \mathbf{Y}_0)]$ .

Note that  $\mathbf{S}_0 = (f'_{\mathbf{X}}(\mathbf{X}_0, \mathbf{Y}_0))^{-1}$ , i.e., the inversion of the Jacobian matrix  $\mathbf{J}_0$ , expressed as

$$\mathbf{J}_{ij0} = \left[ \begin{array}{cc} \frac{\partial P_i}{\partial U_j} & \frac{\partial P_i}{\partial \theta_j} \\ \frac{\partial Q_i}{\partial U_j} & \frac{\partial Q_i}{\partial \theta_j} \end{array} \right] \bigg|_{U_j=U_{j0}, \theta_j=\theta_{j0}}. \quad (41)$$

Thus, we describe the power system operation using a random matrix—if there is an unexpected active power change or short circuit, the corresponding change of system status variables  $\mathbf{X}_0$ , i.e.  $V_i, \theta_i$ , will obey (39) or (40) respectively.

For a practical system, we can always build a relationship in the form of  $\mathbf{Y} = \mathbf{H}\mathbf{X}$  with a similar procedure as (35) to (40); it is linear in high dimensions. For an equilibrium operation system in which the reactive power is almost constant or changes much more slowly than the active one, the relationship model between voltage magnitude and active power is just like the Multiple Input Multiple Output (MIMO) model in wireless communication [49, 78]. Note that most variables of vector  $\mathbf{V}$  are random due to the ubiquitous noises, e.g., small random fluctuations in  $\mathbf{P}$ . In addition, we can add very small artificial fluctuations to make them random or replace the missing/bad data with random Gaussian variables. Furthermore, with the normalization, we can build the standard random matrix model (RMM) in the form of  $\tilde{\mathbf{V}} = \tilde{\mathbf{E}}\mathbf{R}$ , where  $\mathbf{R}$  is a standard Gaussian random matrix.

The data-driven approach conducts analysis requiring no prior knowledge of system topologies, unit operation/control mechanism, causal relationship, etc. It is able to handle massive data all at once; the large size of the data, indeed, enhances the robustness of the final decision against the bad data (errors, losses, or asynchronization). Comparing with classical data-driven methodologies (e.g. PCA), the RMT-based counterpart has some unique characteristics:

- The statistical indicator is generated from all the data in the form of matrix entries. This is not true to principal components—we really do not know the rank of the covariance matrix. Thus, the RMT approach is robust against those challenges in classical data-driven methods, such as error accumulations and spurious correlations [53].
- For the statistical indicator, a theoretical or empirical value can be obtained in advance. The statistical indicator such as LES follows Gaussian distribution, and its variance is bounded [79] and decays very fast in the order of  $O(N^{-2})$  given a moderate data dimension  $N$ , say  $N = 118$ .
- We can flexibly handle heterogenous data to realize data fusion via matrix operations, such as the blocking [80], the sum [78], the product [78], and the concatenation [53] of matrices. Data fusion is guided by the latest mathematical research [49, Chapter 7].
- Only eigenvalues are used for further analyses, while the eigenvectors are omitted. This leads to much smaller required memory space and faster data-processing speed. Although some information is lost in this way, there is still rich information contained in the eigenvalues [81], especially those outliers [82, 83].
- Particularly, for a certain RMM, various forms of LES can be constructed by designing test functions without introducing any physical error (i.e.  $\tau_F = \sum_{i=1}^N \varphi_F(\lambda_{M,i})$ ). Each LES, similar to a filter, provides a unique view-angle. As a result, the system is systematically understood piece by piece. Finally, with a proper LES, we can trace some specific signal.

We adopt a standard IEEE 118-node system as the grid network (Fig. 15) and the events is shown in Tab. I.

TABLE I  
SERIES OF EVENTS

Stage	E1	E2	E3	E4
Time (s)	1–500	501–900	901–1300	1301–2500
$P_{\text{Node-52}}$ (MW)	0	↑ 30	↑ 120	↗ $t/4 - 205$

$P_{52}$  is the power demand of node 52.

The power demand of nodes are assigned as

$$\tilde{y}_{\text{load}_nt} = y_{\text{load}_nt} \times (1 + \gamma_{\text{Mul}} \times r_1) + \gamma_{\text{Acc}} \times r_2, \quad (42)$$

where  $r_1$  and  $r_2$  are the element of standard Gaussian random matrix;  $\gamma_{\text{Acc}}=0.1$ ,  $\gamma_{\text{Mul}}=0.001$ . Thus, the power demand on each node is obtained as the system injections (Fig. 16(a)); the voltage can also be obtained (Fig. 16(b)). Suppose we sample the voltage data at 1 Hz, the data source is denoted as  $\Omega_{\mathbf{V}} : \tilde{v}_{i,j} \in \mathbb{R}^{118 \times 2500}$ . The number of dimensions is  $n = 118$  and the sampling time span is  $t = 2500$ .

Suppose that the power demand data (Fig. 16(a)) are *unknown* or unqualified for SA due to the low sampling frequency or the bad quality. For further analysis, we just start with data source  $\Omega_{\mathbf{V}}$  (Fig. 16(b)) and assign the analysis matrix as  $\mathbf{X} \in \mathbb{R}^{118 \times 240}$  (4 minutes' time span). First, we conduct category for the system operation status; the results are shown as Fig.

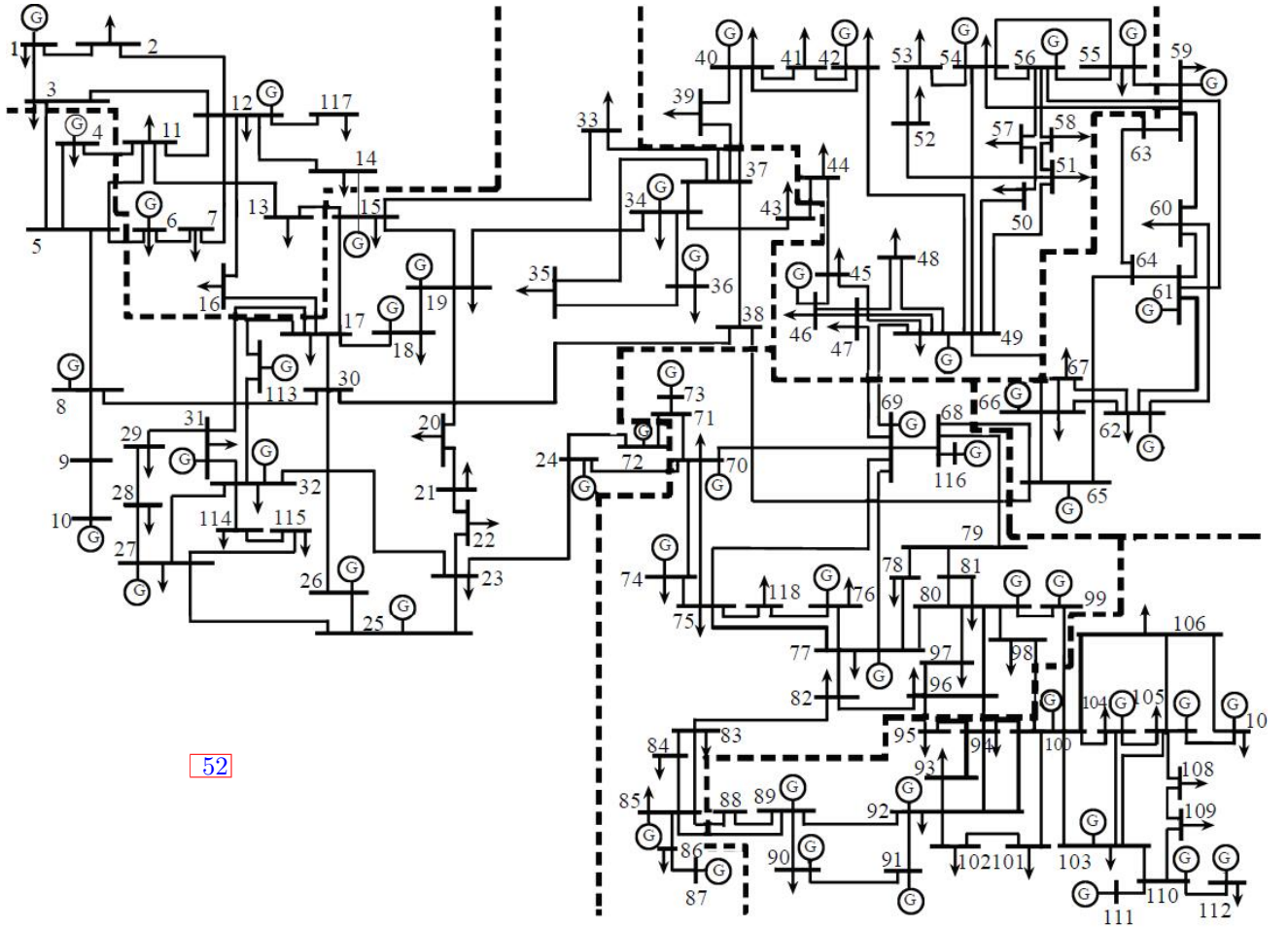


Fig. 15. Partitioning network for the IEEE 118-node system.

16(c). In general, according to the raw data source and the analysis matrix size, we divide our system into 8 stages. Note that it is a statistical division— $S_4$ ,  $S_5$ , and  $S_6$  are transition stages, and their time span is right equal to the length of the analysis matrix minus one, i.e.,  $T-1=239$ . These stages are described as follows:

- For  $S_0, S_1, S_2$ , the white noises play a dominant part.  $P_{\text{Node-52}}$  is rising in turn.
- For  $S_3$ ,  $P_{\text{Node-52}}$  maintains stable growth.
- $S_4$ , transition stage. Ramping signal exists.
- $S_5, S_6$ , transition stages. Step signal exists.
- For  $S_7$ , voltage collapse.

We also select two typical data cross-sections for stage  $S_0$  and  $S_6$ :  $X_0 \in \mathbb{R}^{118 \times 240}$  during period  $t = [61 : 300]$  at the sampling time  $t_{\text{end}}=300$ , and 2)  $X_6 \in \mathbb{R}^{118 \times 240}$  during period  $t = [662 : 901]$  at the sampling time  $t_{\text{end}}=901$ .

Besides, as discussed in II-A, we build up the RMM  $\hat{V}$  from the raw voltage data. Then,  $\tau_{\text{MSR}}$  is employed as a statistical indicator to conduct anomaly detection. For the selected data cross-section  $X_0$  and  $X_6$ , their M-P Law and Ring Law Analysis are shown as Fig 17(a), 17(b), 17(c) and 17(d).

Fig 17 shows that when there is no signal in the system, the experimental RMM well matches Ring Law and M-P Law, and the experimental value of LES is approximately equal to the theoretical value. This validates the theoretical justification for modeling rapid fluctuation at each node with additive white Gaussian noise, as shown in Section II-A. On the other hand, Ring Law and M-P Law are violated at the very beginning ( $t_{\text{end}}=901$ ) of the step signal. Besides, the proposed high-dimensional indicator  $\tau_{\text{MSR}}$ , is extremely sensitive to the anomaly. At  $t_{\text{end}}=901$ , the  $\tau_{\text{MSR}}$  starts the dramatic change as shown in the  $\tau_{\text{MSR}}-t$  curve, while the raw voltage magnitudes remain still in the normal range as shown in Fig. 16(c). Moreover, we design numerous kinds of LES  $\tau$  and define  $\mu_0 = \tau / \mathbb{E}(\tau)$ . The results are shown in Fig. 18 and prove that different indicators have different characteristics and effectiveness; this suggests another topic to explore in the future.

Furthermore, we investigate the SA based on the high dimensional spectrum test. The sampling time is set as  $t_{\text{end}}=300$  and  $t_{\text{end}}=901$ . Following Lemma II.7 and Lemma II.9,

$Y_0, Y_6 \in \mathbb{R}^{118 \times 240}$  (span  $t = [61 : 300]$  and  $t = [662 : 901]$ ), and  $Z_0, Z_6 \in \mathbb{R}^{118 \times 118}$  (span  $t = [183 : 300]$  and  $t = [784 : 901]$ ) are

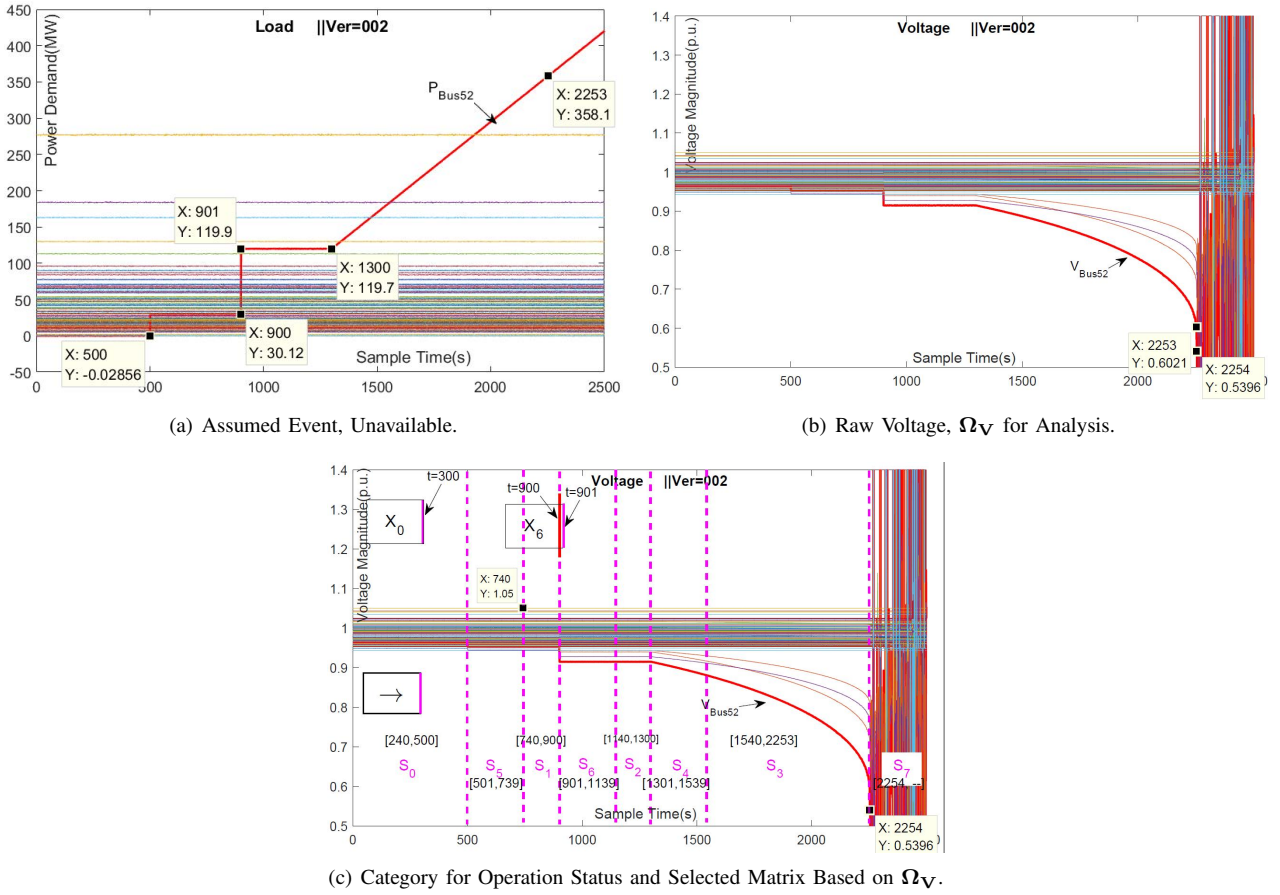


Fig. 16. Assumed Event, Data Source, and Category for Case.

selected. The results are shown in Fig. 19 and Fig. 20. These results validate that empirical spectral density test is competent to conduct anomaly detection—when the power grid is under a normal condition, the empirical spectral density  $f_A(x)$  and the ESD function  $F_A(x)$  are almost strictly bounded between the upper bound and the lower bound of their asymptotic limits. On the other hand, these results also validate that GUE and LUE are proper mathematical tools to model the power grid operation.

The  $V - P$  curve (also called nose curve) and the smallest eigenvalue of the Jacobian matrix [39] are two clues for steady stability evaluation. In this case, we focus on the E4 part during which  $P_{\text{Node-52}}$  keep increasing to break down the steady stability. The related  $V - P$  curve and  $\lambda - P$  curve, respectively, are given in Fig. 21(a) and Fig. 21(b). Only using the data source  $\Omega_V$ , we choose some data cross-section,  $T_1: [1601:1840]$ ;  $T_2: [1901:2140]$ ;  $T_3: [2101:2340]$ , as shown in Fig. 21(a). The RMT-based results are shown as Fig. 22. The outliers become more evident as the stability degree decreases. The statistics of the outliers are similar to the smallest eigenvalue of Jacobian Matrix, Lyapunov Exponent or the entropy in some sense.

For further analysis, we take the signal and stage division into account. Generally speaking, sorted by the stability degree, the stages are ordered as  $S_0 > S_1 > S_2 > S_3 \gg \max(S_4, S_5) \gg S_6 \gg S_7$ . According to Fig. 18, we make the Table II. The high-dimensional indicators  $\overline{\tau_{X_R}}$  and  $V_R$  have the same trend as the stability degree order. These statistics have the potential for data-driven stability evaluation.

The key for correlation analysis is the concatenated matrix  $A_i$ , which consist of two part—the basic matrix  $B$  and a certain factor matrix  $C_i$ , i.e.,  $A_i = [B; C_i]$ . For more details, see our previous work [53]. The LES of each  $A_i$  is computed in parallel, and Fig. 23 shows the results.

In Fig. 23, the blue dot line (marked with None) shows the LES of basic matrix  $B$ , and the orange line (marked with Random) shows the LES of the concatenated matrix  $[B; R]$  ( $R$  is the standard Gaussian Random Matrix). Fig. 23 demonstrates that: 1) node 52 is the causing factor of the anomaly; 2) sensitive nodes are 51, 53, and 58; and 3) nodes 11, 45, 46, etc, are not affected by the anomaly. Based on this algorithm, we can continue to conduct behavior analysis, e.g., detection and estimation of residential PV installations [84]. Behavior analysis is a big topic. Limited to the space, we will not expand it here.

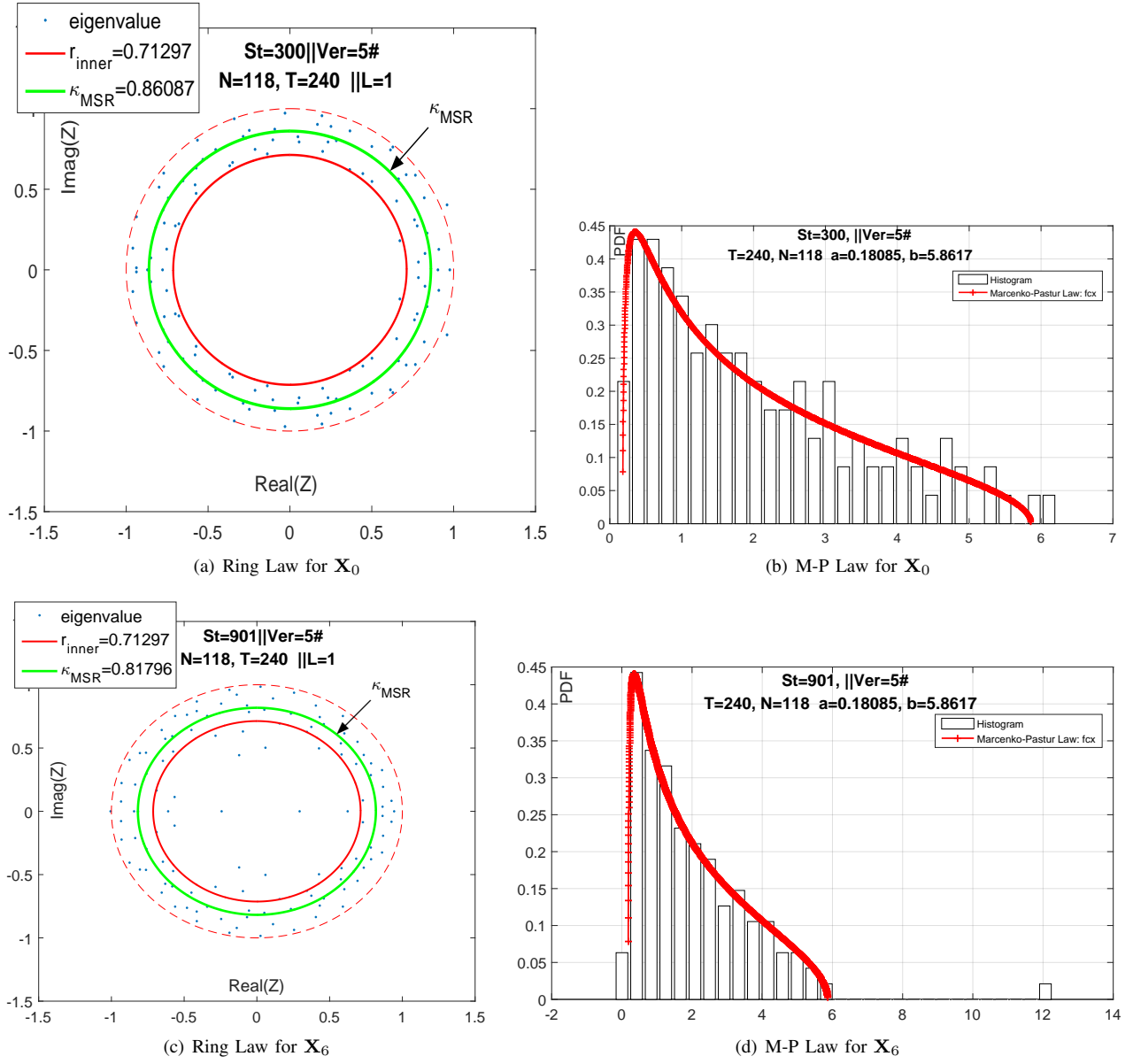


Fig. 17. Anomaly Detection Result.

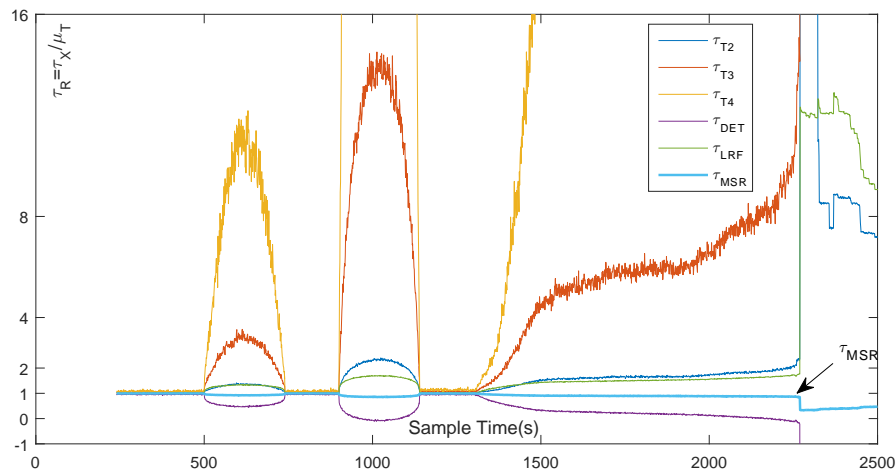


Fig. 18. Illustration of Various LES Indicators.

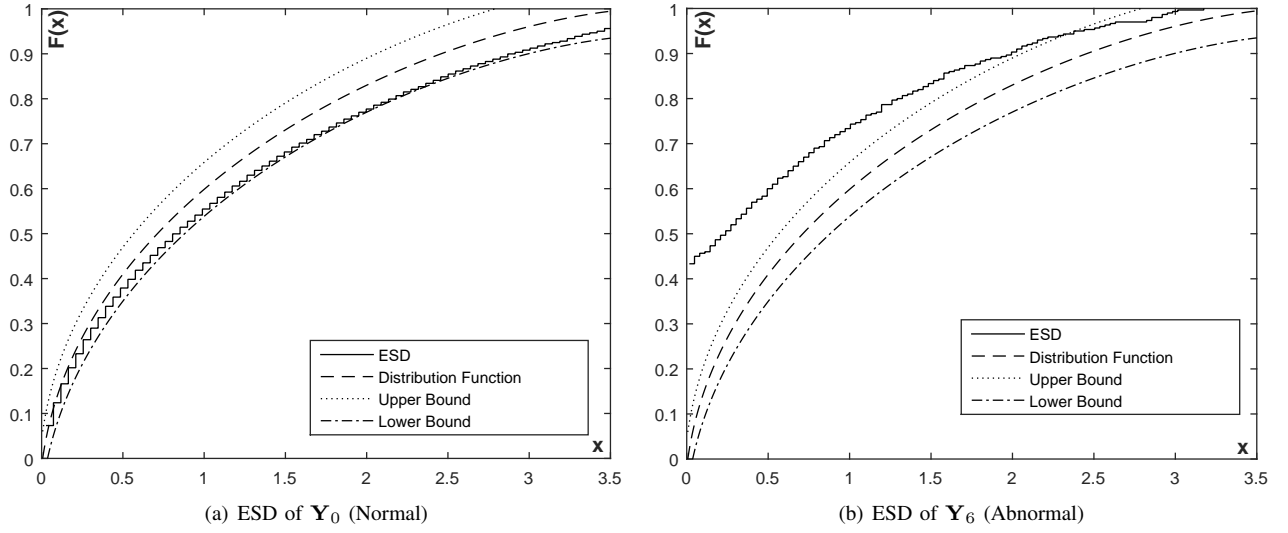


Fig. 19. Anomaly Detection Using LUE matrices

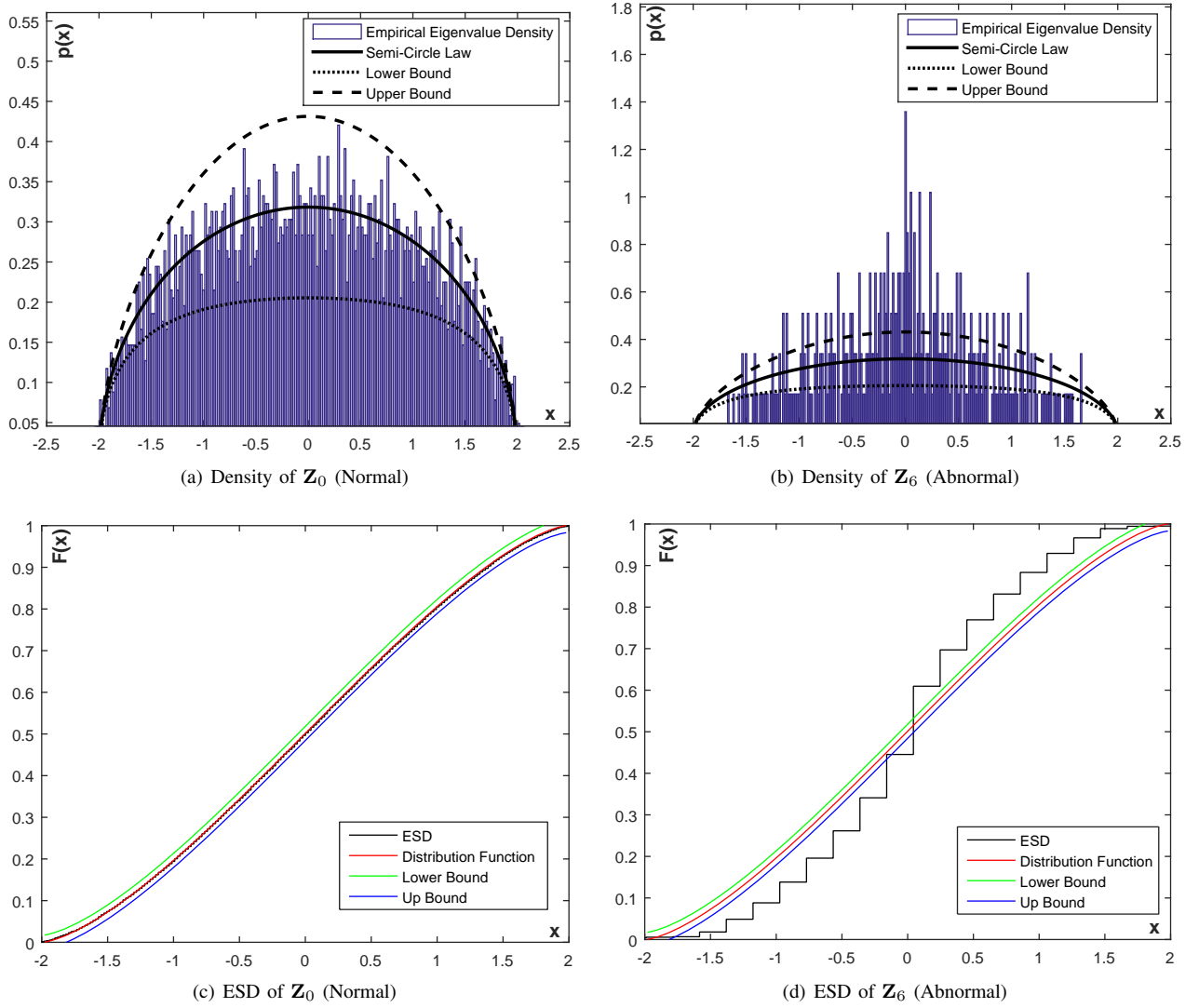


Fig. 20. Anomaly Detection Using GUE matrices

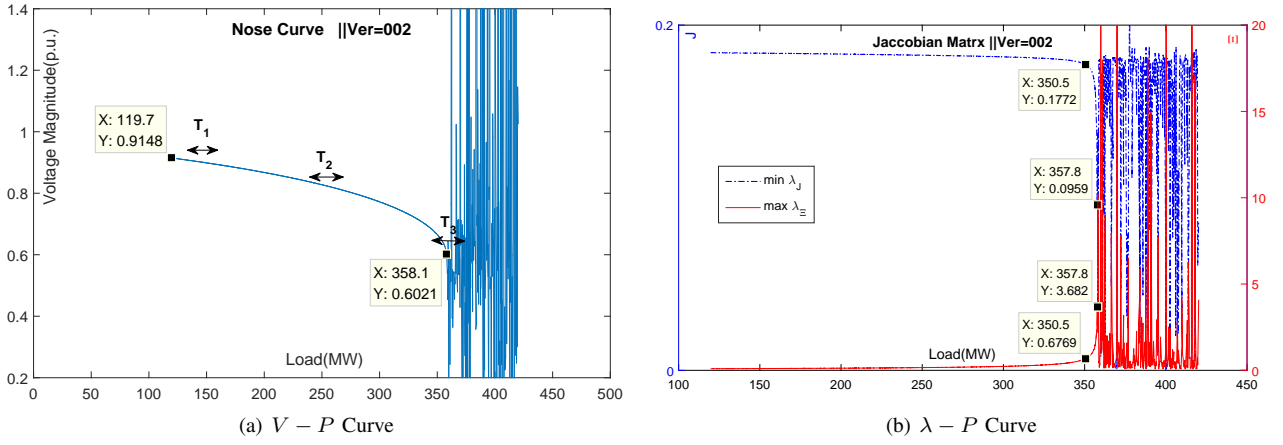


Fig. 21. The  $V - P$  curve and  $\lambda - P$  curve.

TABLE II  
INDICATOR OF VARIOUS LESS AT EACH STAGE.

	MSR	$T_2$	$T_3$	$T_4$	DET	LRF
<b>E<sub>0</sub>: Theoretical Value</b>						
$\mathbb{E}(\tau)$	0.8645	1338.3	10069	8.35E4	48.322	73.678
$\mathbb{D}_T(\tau)$	—	665.26	93468	1.30E7	1.3532	1.4210
<b>S0 [0240:0500, 261]: Small fluctuations around 0 MW</b>						
$\bar{\tau}_{\mathbf{X}_R}$	0.995	1.010	1.040	1.080	0.959	1.014
$V$	6E-6	78.38	3.03E4	7.14E6	0.4169	0.3908
$V_R$	1	1	1	1	1	1
<b>S5 [0501:0739, 239]: A step signal (0 MW <math>\uparrow</math> 30 MW) is included</b>						
$\bar{\tau}_{\mathbf{X}_R}$	0.9331	1.280	2.565	7.661	0.5453	1.284
$V_R$	1.49E1	1.64E2	1.16E3	8.63E3	3.43E1	3.97E1
<b>S1 [0740:0900, 161]: Small fluctuations around 30 MW</b>						
$\bar{\tau}_{\mathbf{X}_R}$	0.9943	1.010	1.039	1.084	0.9568	1.015
$V_R$	0.8608	0.9121	0.9476	1.234	0.8972	1.101
<b>S6 [0901:1139, 239]: A step signal (30 MW <math>\uparrow</math> 120 MW) is included</b>						
$\bar{\tau}_{\mathbf{X}_R}$	0.8742	2.054	1.06E1	7.22E1	7E-2	1.597
$V_R$	5.49E1	2.06E3	3.87E4	8.54E5	1.52E2	1.62E2
<b>S2 [1140:1300, 161]: Small fluctuations around 120 MW</b>						
$\bar{\tau}_{\mathbf{X}_R}$	0.9930	1.019	1.067	1.135	0.9488	1.021
$V_R$	0.7823	1.053	1.189	1.135	0.7310	0.9255
<b>S4 [1301:1539, 239]: A ramp signal (119.7 MW <math>\nearrow</math>) is included</b>						
$\bar{\tau}_{\mathbf{X}_R}$	0.9337	1.295	2.787	9.615	0.5316	1.294
$V_R$	8.50E1	7.41E2	5.63E3	5.17E4	2.14E2	2.30E2
<b>S3 [1540:2253, 714]: Steady increase (<math>\nearrow</math> 358.1 MW)</b>						
$\bar{\tau}_{\mathbf{X}_R}$	0.8906	1.717	6.530	3.48E1	0.1483	1.545
$V_R$	1.35E1	3.28E2	5.33E3	1.10E5	6.11E1	6.85E1
<b>S7 [2254:2500, 247]: Static voltage collapse (361.9 MW <math>\nearrow</math>)</b>						
$\bar{\tau}_{\mathbf{X}_R}$	0.4259	1.02E1	2.11E2	4.65E3	-1.4E1	1.08E1
$V_R$	1.94E3	5.81E5	1.20E8	3.2E10	9.02E4	9.62E4

\* $\bar{\tau}_{\mathbf{X}_R} = \bar{\tau}_{\mathbf{X}}/\mathbb{E}(\tau)$ ;  $V_R(\tau_{\mathbf{X}}) = V(\tau_{\mathbf{X}})/V(\tau_{\mathbf{X}_0})$ .

#### D. Early Event Detection using Free Probability

**Problem Modeling :** Following [85], we build the statistic model for power grid. Considering  $T$  random vectors observed at time instants  $i = 1, \dots, T$ , we form a random matrix as follows

$$[\Delta \mathbf{V}_1, \dots, \Delta \mathbf{V}_T] = [\Xi_1 \Delta \mathbf{P}_1, \dots, \Xi_T \Delta \mathbf{P}_T]. \quad (43)$$

In an equilibrium operating system, the voltage magnitude vector injections  $\mathbf{V}$  with entries  $V_i, i = 1, \dots, N$  and the phase angle vector injections  $\boldsymbol{\theta}$  with entries  $\theta_i, i = 1, \dots, N$  experience slight changes. Without dramatic topology changes, rich statistical empirical evidence indicates that the Jacobian matrix  $\mathbf{J}$  keeps nearly constant, so does  $\Xi$ . Also, we can estimate the changes of  $\mathbf{V}$ ,  $\boldsymbol{\theta}$ , and  $\Xi$  only with the classical approach. Thus we rewrite (43) as:



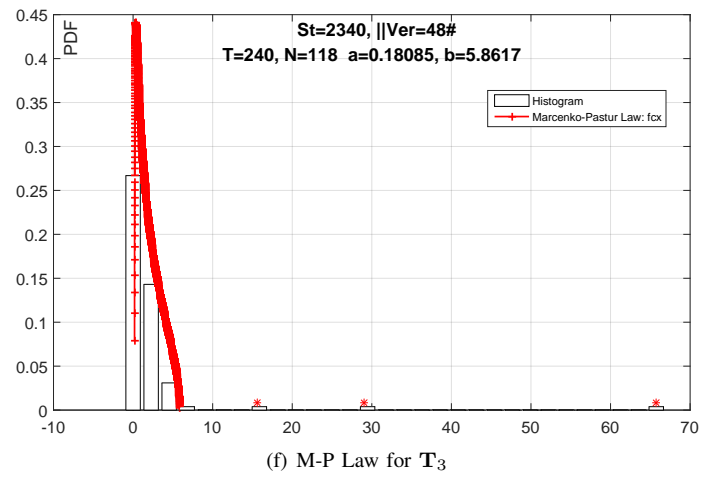
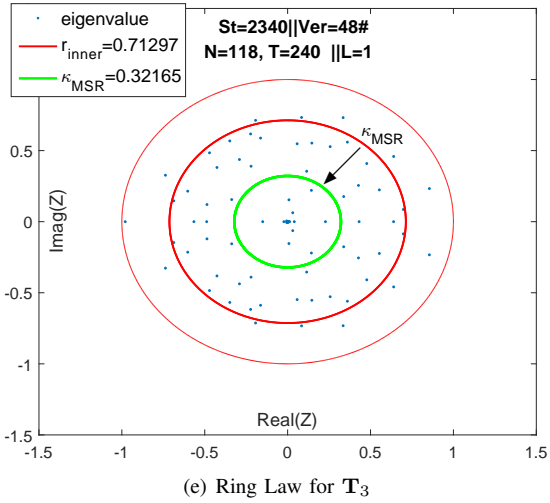
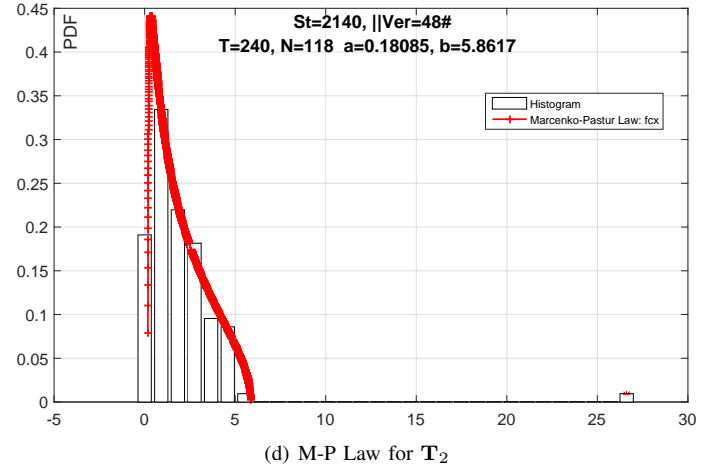
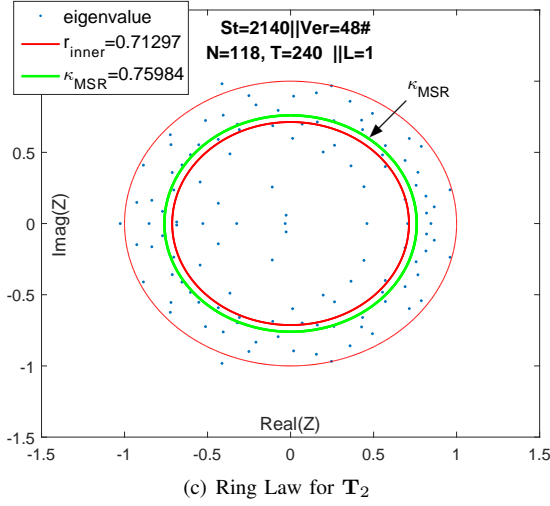
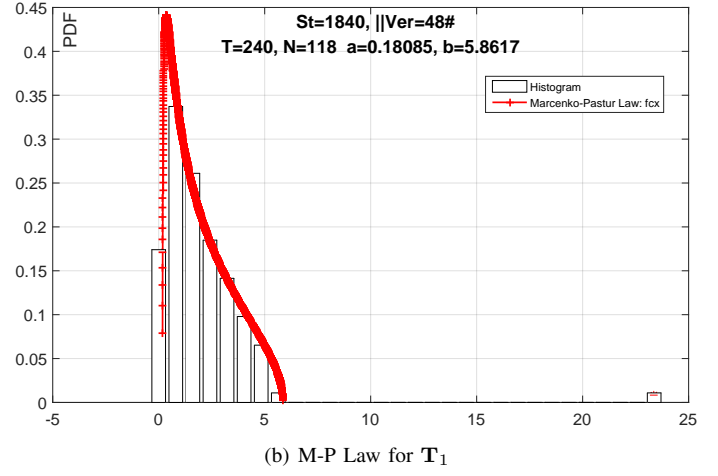
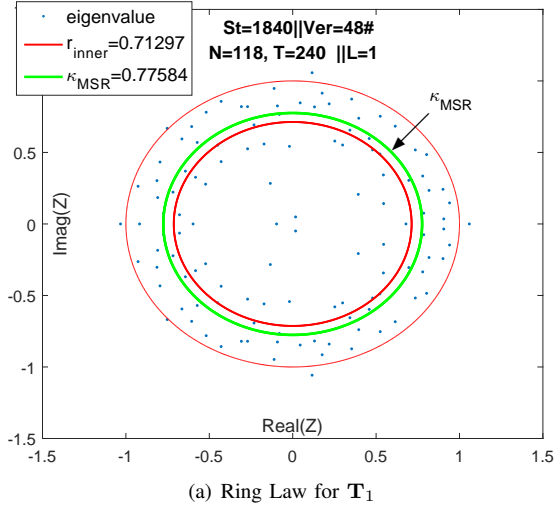


Fig. 22. RMT-based Results for Voltage Stability Evaluation.



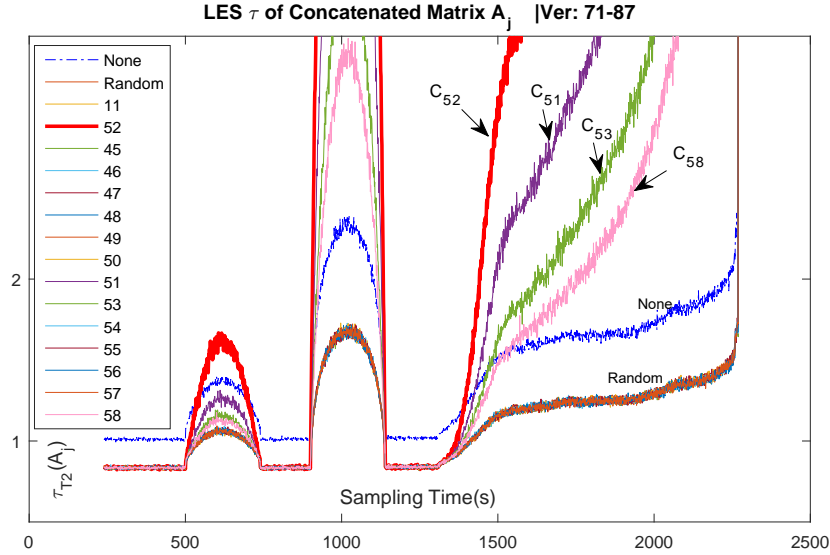


Fig. 23. Sensitivity Analysis based on Concatenated Matrix.

$$\mathbb{V} = \Xi_N \mathbb{P}_{N \times T} \quad (44)$$

where  $\mathbb{V} = [\Delta \mathbf{V}_1, \dots, \Delta \mathbf{V}_T]$ ,  $\Xi = \Xi_1 = \dots = \Xi_T$ , and  $\mathbb{P} = [\Delta \mathbf{P}_1, \dots, \Delta \mathbf{P}_T]$ . Here  $\mathbb{V}$  and  $\mathbb{P}$  are random matrices. In particular,  $\mathbb{P}$  is a random matrix with Gaussian entries.

**Model Designs :** Multivariate linear or nonlinear polynomials perform a significant role in problem modeling, so we build our models on the basis of random matrix polynomials. Here, we study two typical random matrix polynomial models.

The first case is the multivariate linear polynomial:

$$P_1(S_0, S_1) = S_0 + S_1.$$

The second one is the selfadjoint multivariate nonlinear polynomial:

$$P_2(S_0, S_1) = S_0 S_1 + S_1 S_0.$$

Here, both  $S_0$  and  $S_1$  are the sample covariance matrices. The asymptotic eigenvalue distributions of  $P_1$  and  $P_2$  can be obtained via basic principles of the free probability theory as introduced above. The asymptotic eigenvalue distributions of  $P_i$  are regarded as the theoretical bounds.

#### Hypothesis Testing and Anomaly Detection :

We formulate our problem of anomaly detection in terms of the same hypothesis testing as [85]: no outlier exists  $\mathcal{H}_0$ , and outlier exists  $\mathcal{H}_1$ .

$$\left| \begin{array}{l} \mathcal{H}_0 : \tilde{\mathbb{V}} = \tilde{\Xi} R_{N \times T} \\ \mathcal{H}_1 : \tilde{\mathbb{V}} \neq \tilde{\Xi} R_{N \times T} \end{array} \right. \quad (45)$$

where  $R$  is the standard Gaussian random matrix.

Generate  $S_0, S_1$  from the sample data through the preprocess in III-D . Compare the theoretical bound with the spectral distribution of raw data polynomials. If outlier exists,  $\mathcal{H}_0$  will be rejected, i.e. signals exist in the system.

**The Processing of the Grid Data :** The data sampled from power grid is always non-Gaussian, so we adopt a normalization procedure in [80] to conduct data preprocessing. Meanwhile, we employ Monte Carlo method to compute the spectral distribution of raw data polynomial according to the asymptotic property theory. See details in Algorithm.1.

#### Simulation Results :

Our data fusion method is tested with simulated data in the standard IEEE 118-bus system. Detailed information of the system is referred to the case118.m in Matpower package and Matpower 4.1 User's Manual [86]. For all cases, let the sample dimension  $N = 118$ . In our simulations, we set the sample length equal to  $N$ , i.e.  $T = 118$ ,  $c = T/N = 1$  and select six sample voltage matrices presented in Tab. III, as shown in Fig. 24. The results of our simulations are presented in Fig. 25 and Fig. 26. The outliers existed when the system was abnormal and its sizes become large when the anomaly become serious.

**Algorithm 1****Require:**The sample data matrices:  $V_0$  and  $V_1$  ;The number of repetition times :  $M$ ;The size of  $V_0$  and  $V_1$ :  $N, T$ ;SNR:  $\eta$ 1: **for**  $i \leq M$  **do**

2:   add small white noises to sample data matrices

$$\widetilde{V}_0 = V_0 + \eta \text{ randn}(N, N);$$

$$\widetilde{V}_1 = V_0 + \eta \text{ randn}(N, N);$$

3:   standardize  $\widetilde{V}_0$  and  $\widetilde{V}_1$ , i.e. mean=0, variance=1;4:   generate the covariance matrices:  $S_0 = \widetilde{V}_0 \widetilde{V}_0' / N$ ,

$$S_0 = \widetilde{V}_1 \widetilde{V}_1' / N;$$

5:   compute the eigenvalues of  $P(S_0, S_1)$ ;6: **end for**

7: Computer the frequency of different eigenvalues and draw the spectral distribution histogram;

**Ensure:**

The spectral distribution histogram.

TABLE III  
SYSTEM STATUS AND SAMPLING DATA

Cross Section (s)	Sampling (s)	Descripton
$C_0$ : 118 – 900	$V_0$ : 100 ~ 217	Reference, no signal
$C_1$ : 901 – 1017	$V_1$ : 850 ~ 967	Existence of a step signal
$C_2$ : 1918 – 2600	$V_2$ : 2200 ~ 2317	Steady load growth for Bus 22
$C_3$ : 3118 – 3790	$V_3$ : 3300 ~ 3417	Steady load growth for Bus 52
$C_4$ : 3908 – 4100	$V_4$ : 3900 ~ 4017	Chaos due to voltage collapse
$C_5$ : 4118 – 5500	$V_5$ : 4400 ~ 4517	No signal

\*We choose the temporal end edge of the sampling matrix as the marked time for the cross section. E.g., for  $V_0$  : 100 ~ 217, the temporal label is 217 which belong to  $C_0$  : 118 – 800. Thus, this method is able to be applied to conduct real-time analysis.

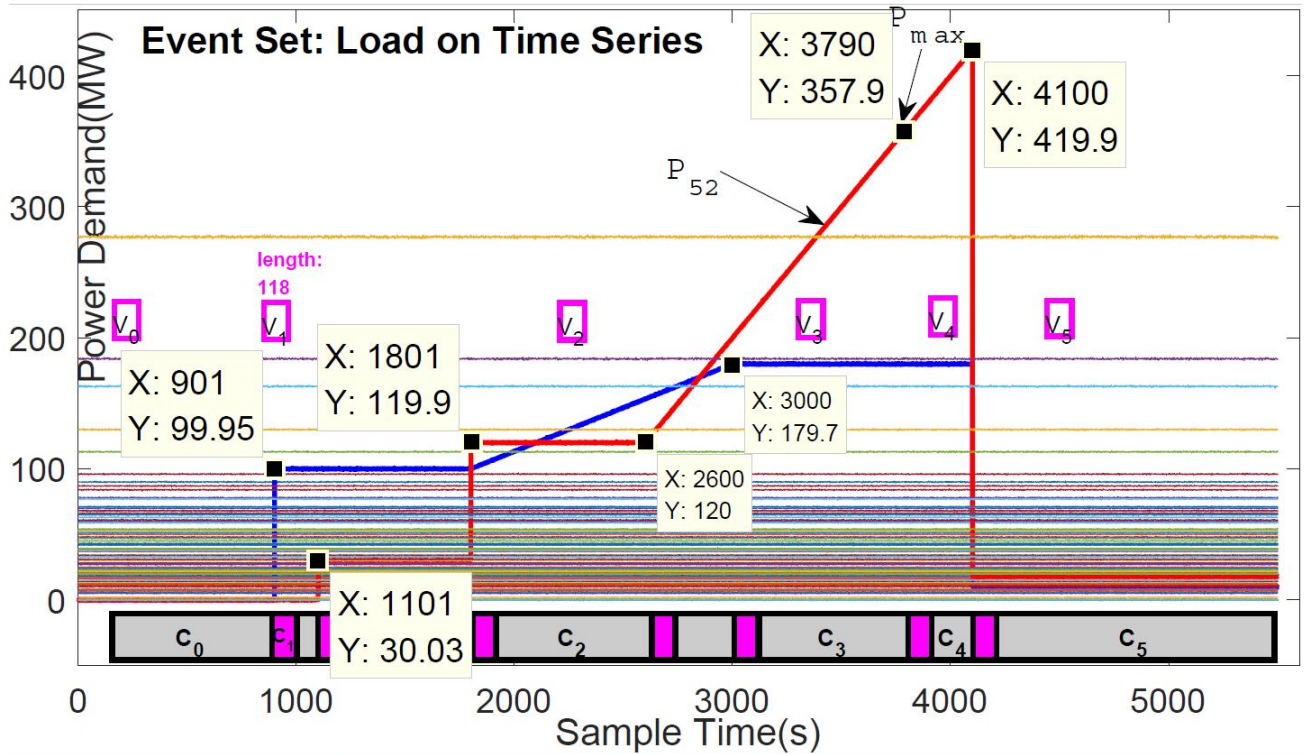
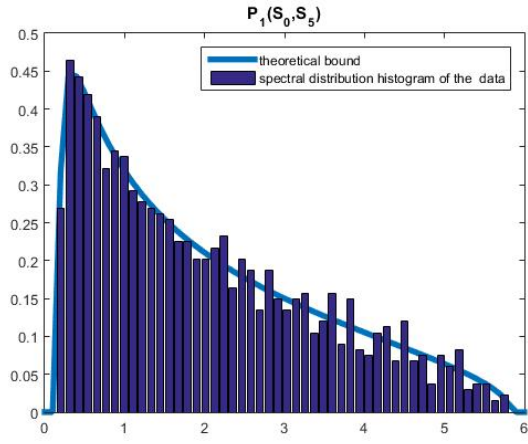
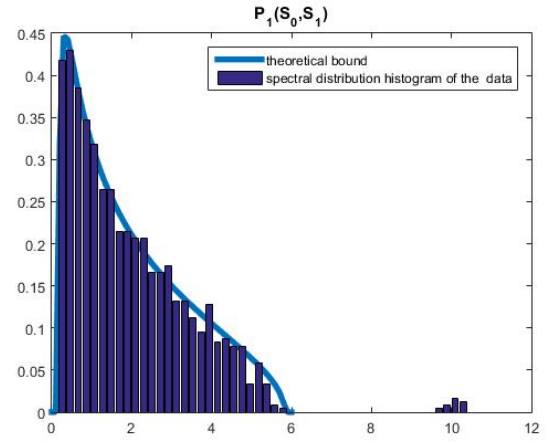
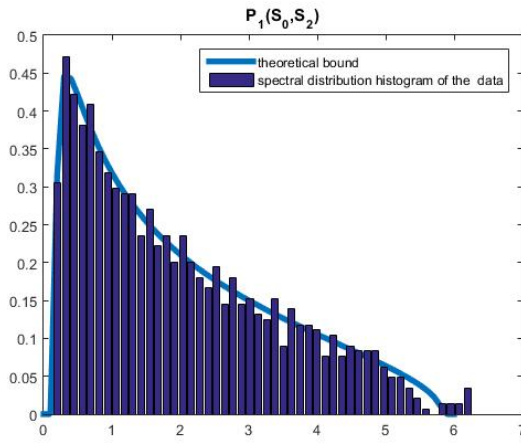
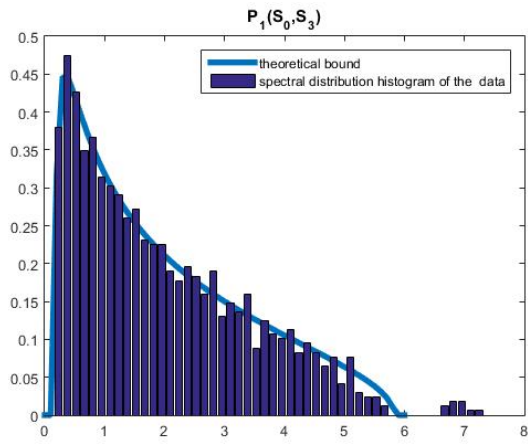
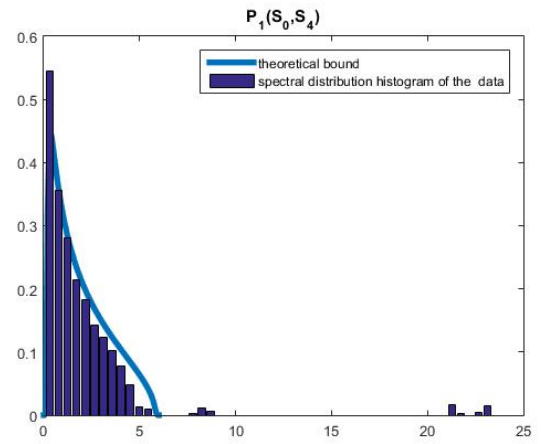
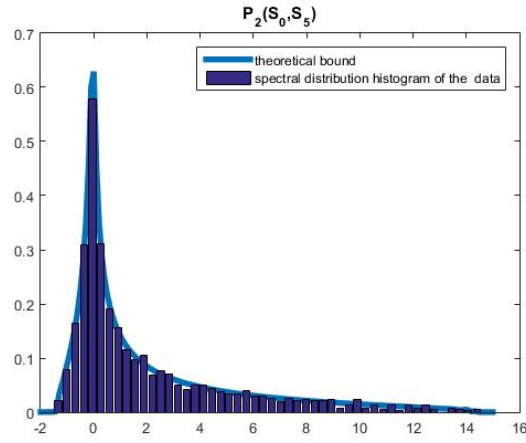
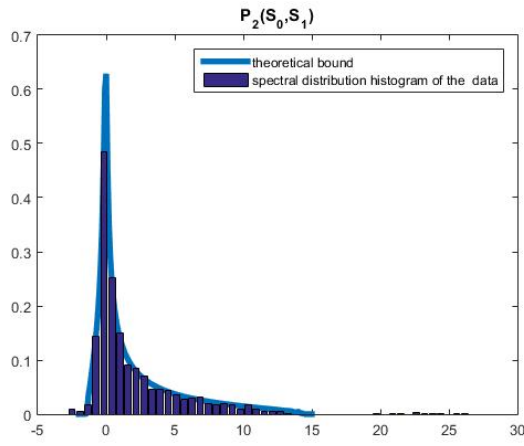
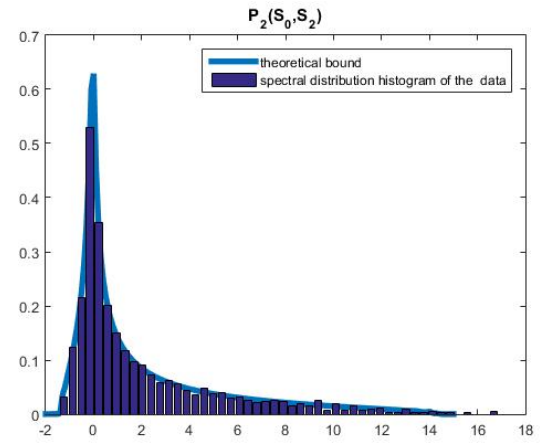
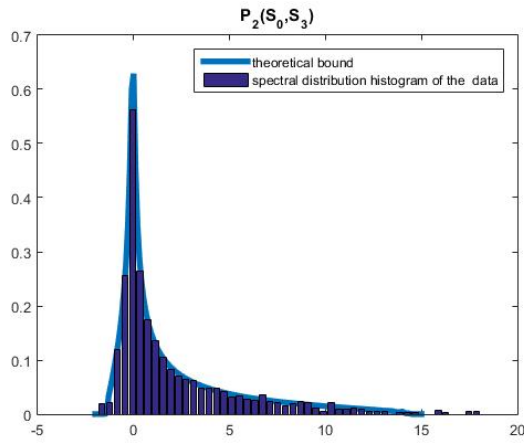
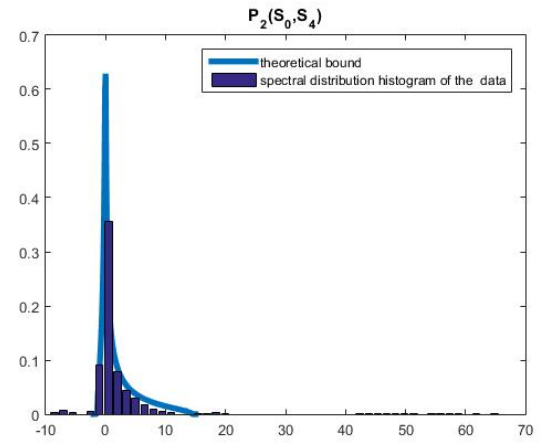


Fig. 24. The event assumptions on time series.

(a) White noises  $V_5$  &  $V_0$ (b) Step signal  $V_1$  &  $V_0$ (c) Stable growth A  $V_2$  &  $V_0$ (d) Stable growth B  $V_3$  &  $V_0$ (e) Voltage collapse  $V_4$  &  $V_0$ Fig. 25. Data fusion using multivariate linear polynomial  $P_1$

(a) White noises  $V_5$  &  $V_0$ (b) Step signal  $V_1$  &  $V_0$ (c) Stable growth A  $V_2$  &  $V_0$ (d) Stable growth B  $V_3$  &  $V_0$ (e) Voltage collapse  $V_4$  &  $V_0$ Fig. 26. Data fusion using multivariate nonlinear polynomial  $P_2$ .

#### IV. CONCLUSION AND FUTURE DIRECTIONS

Motivated by the immediate demands of tackling the tricky problems raised from large scale smart grids, this chapter introduced RMT-based schemes for spatio-temporal big data analysis. Firstly, we represent the spatio-temporal PMU data as a sequence of large random matrices. This is a crucial part for power state evaluation as it turning the big PMU data into tiny data for the practical use. Rather than employing the raw PMU data, a comprehensive analysis of PMU data flow, namely, RMT-based techniques, is then proposed to indicate the state evaluation state. The core techniques include streaming PMU data modelling, asymptotic properties analysis and data fusion methods (based on free probability). Besides, the case studies based on synthetic data and real data are also included with the aim to bridge the technology gap between RMT and spatio-temporal data analysis in smart grids.

The current works based on RMT, provides a fundamental exploration of data analysis for spatio-temporal PMU data. Much more attentions are to be paid along this research direction, such as classification of power events and load forecasting. It is also noted that this work provide data-driven methods which are new substitutes for power system state estimation. The combination of power system scenario analysis, spectrum sensing mechanisms, networking protocols and big data techniques [15, 34, 49, 87] is encouraged to be investigated for better understanding of the power system state.

#### REFERENCES

- [1] US DOE. Grid 2030: A national vision for electricity's second 100 years. US DOE Report, 2003.
- [2] Santiago Grijalva and Muhammad Umer Tariq. Prosumer-based smart grid architecture enables a flat, sustainable electricity industry. In Innovative Smart Grid Technologies (ISGT), 2011 IEEE PES, pages 1–6. IEEE, 2011.
- [3] Xiaoxin Zhou, Shuyong Chen, and Zongxiang Lu. Review and prospect for power system development and related technologies: a concept of three-generation power systems. Proceedings of the CSEE, 33(22):1–11, Aug. 2013.
- [4] Shengwei Mei, Yuan Gong, and Feng LIU. The evolution model of three generation power systems and characteristic analysis. Proceedings of the CSEE, 7:1003–1012, 2014.
- [5] Xing He, Qian Ai, Zhiwen Yu, Yiting Xu, and Jian Zhang. Power system evolution and aggregation theory under the view of power ecosystem. Power System Protection and Control, 42(22):100–107, Nov. 2014.
- [6] Zhang Hong, Dongmei Zhao, Chenghong Gu, Furong Li, and Bo Wang. Economic optimization of smart distribution networks considering real-time pricing. Journal of Modern Power Systems and Clean Energy, 2(4):350–356, 2014.
- [7] Yang Ji. Multi-agent system based control of virtual power plant and its application in smart grid. Master's thesis, School of Electronic Information and Electrical Engineering, Shanghai Jiaotong University, 2011.
- [8] Xing He, Qian Ai, Peng Yuan, and Xiaohong Wang. The research on coordinated operation and cluster management for multi-microgrids. In Sustainable Power Generation and Supply (SUPERGEN 2012), International Conference on, pages 1–3. IET, 2012.
- [9] Wilsun Xu and Jing Yong. Power disturbance data analytics—new application of power quality monitoring data. Proceedings of the CSEE, 33(19):93–101, July 2013.
- [10] IBM. The Four V's of Big Data. accessed date: July, 2015.
- [11] LS Moulin, AP Alves da Silva, MA El-Sharkawi, et al. Support vector machines for transient stability analysis of large-scale power systems. Power Systems, IEEE Transactions on, 19(2):818–825, 2004.
- [12] Yael Parag and Benjamin K Sovacool. Electricity market design for the prosumer era. Nature Energy, 1:16032, 2016.
- [13] C. Lynch. Big data: How do your data grow? Nature, 455(7209):28, 2008.
- [14] Science Staff. Dealing with data. challenges and opportunities. introduction. Science, 331(6018):692, 2011.
- [15] A. A Khan, M. H Rehmani, and M Reisslein. Cognitive radio for smart grids: Survey of architectures, spectrum sensing mechanisms, and networking protocols. IEEE Communications Surveys and Tutorials, 18(1):1–1, 2015.
- [16] Lei Chu, Robert Caiming Qiu, Xing He, Zenan Ling, and Yadong Liu. Massive streaming pmu data modeling and analytics in smart grid state evaluation based on multiple high-dimensional covariance tests. IEEE Transactions on Big Data, PP(99):1–1, 2017.
- [17] Tómas A Brody, J Flores, J Bruce French, PA Mello, A Pandey, and Samuel SM Wong. Random-matrix physics: spectrum and strength fluctuations. Reviews of Modern Physics, 53(3):385–480, 1981.
- [18] Laurent Laloux, Pierre Cizeau, Marc Potters, and Jean-Philippe Bouchaud. Random matrix theory and financial correlations. International Journal of Theoretical and Applied Finance, 3(3):391–397, July 2000.
- [19] Hsinchun Chen, Roger HL Chiang, and Veda C Storey. Business intelligence and analytics: From big data to big impact. MIS quarterly, 36(4):1165–1188, 2012.
- [20] Doug Howe, Maria Costanzo, Petra Fey, Takashi Gojobori, Linda Hannick, Winston Hide, David P Hill, Renate Kania, Mary Schaeffer, Susan St Pierre, et al. Big data: The future of biocuration. Nature, 455(7209):47–50, 2008.
- [21] Robert Qiu and Michael Wicks. Cognitive Networked Sensing and Big Data. Springer, 2013.
- [22] C. Zhang and R. C. Qiu. Data modeling with large random matrices in a cognitive radio network testbed: Initial experimental demonstrations with 70 nodes. ArXiv e-prints, Apr. 2014.

- [23] Xia Li, Feng Lin, and Robert C Qiu. Modeling massive amount of experimental data with large random matrices in a real-time UWB-MIMO system. *ArXiv e-prints*, Apr. 2014.
- [24] T. Hong, C. Chen, J. Huang, et al. Guest editorial big data analytics for grid modernization. *IEEE Transactions on Smart Grid*, 7(5):2395–2396, Sept 2016.
- [25] M. Rafferty, X. Liu, D. M. Lavery, and S. McLoone. Real-time multiple event detection and classification using moving window pca. *IEEE Transactions on Smart Grid*, 7(5):2537–2548, Sept 2016.
- [26] H. Jiang, X. Dai, D. W. Gao, J. J. Zhang, Y. Zhang, and E. Muljadi. Spatial-temporal synchrophasor data characterization and analytics in smart grid fault detection, identification, and impact causal analysis. *IEEE Transactions on Smart Grid*, 7(5):2525–2536, Sept 2016.
- [27] H. Sun, Z. Wang, J. Wang, Z. Huang, N. Carrington, and J. Liao. Data-driven power outage detection by social sensors. *IEEE Transactions on Smart Grid*, 7(5):2516–2524, Sept 2016.
- [28] X. Zhang and S. Grijalva. A data-driven approach for detection and estimation of residential pv installations. *IEEE Transactions on Smart Grid*, 7(5):2477–2485, Sept 2016.
- [29] H. Shaker, H. Zareipour, and D. Wood. A data-driven approach for estimating the power generation of invisible solar sites. *IEEE Transactions on Smart Grid*, 7(5):2466–2476, Sept 2016.
- [30] B. Wang, B. Fang, Y. Wang, H. Liu, and Y. Liu. Power system transient stability assessment based on big data and the core vector machine. *IEEE Transactions on Smart Grid*, 7(5):2561–2570, Sept 2016.
- [31] AG Phadke and Rui Menezes de Moraes. The wide world of wide-area measurement. *Power and Energy Magazine, IEEE*, 6(5):52–65, 2008.
- [32] Vladimir Terzija, Gustavo Valverde, Deyu Cai, Pawel Regulski, Vahid Madani, John Fitch, Srdjan Skok, Miroslav M Begovic, and Arun Phadke. Wide-area monitoring, protection, and control of future electric power networks. *Proceedings of the IEEE*, 99(1):80–93, 2011.
- [33] Le Xie, Yang Chen, and Huaiwei Liao. Distributed online monitoring of quasi-static voltage collapse in multi-area power systems. *Power Systems, IEEE Transactions on*, 27(4):2271–2279, 2012.
- [34] Athar Ali Khan, Mubashir Husain Rehmani, and Martin Reisslein. Requirements, design challenges, and review of routing and mac protocols for cr-based smart grid systems. *IEEE Communications Magazine*, 55(5):206–215, 2017.
- [35] Quanyuan Jiang, Xingpeng Li, Bo Wang, and Haijiao Wang. Pmu-based fault location using voltage measurements in large transmission networks. *Power Delivery, IEEE Transactions on*, 27(3):1644–1652, 2012.
- [36] Mahesh Venugopal and Chetan Tiwari. A novel algorithm to determine fault location in a transmission line using pmu measurements. In *Smart Instrumentation, Measurement and Applications (ICSIMA), 2013 IEEE International Conference on*, pages 1–4. IEEE, 2013.
- [37] Ali H Al-Mohammed and MA Abido. A fully adaptive pmu-based fault location algorithm for series-compensated lines. *Power Systems, IEEE Transactions on*, 29(5):2129–2137, 2014.
- [38] Le Xie, Yang Chen, and PR Kumar. Dimensionality reduction of synchrophasor data for early event detection: Linearized analysis. *IEEE Transactions on Power Systems*, 29(6):2784–2794, 2014.
- [39] Jong Min Lim and Christopher L DeMarco. Svd-based voltage stability assessment from phasor measurement unit data. *IEEE Transactions on Power Systems*, 31(4):2557–2565, 2016.
- [40] Eugene P Wigner. Lower limit for the energy derivative of the scattering phase shift. *Physical Review*, 98(1):145, 1955.
- [41] Eugene P. Wigner. On the distribution of the roots of certain symmetric matrices. *Annals of Mathematics*, 67(2):325–327, 1958.
- [42] Eugene P Wigner. The problem of measurement. *American Journal of Physics*, 31(1):6–15, 1963.
- [43] Eugene P. Wigner. Random matrices in physics. *Siam Review*, 9(1):1–23, 1967.
- [44] Eugene P. Wigner. *Characteristic Vectors of Bordered Matrices with Infinite Dimensions I*. Springer Berlin Heidelberg, 1993.
- [45] V. A. Marchenko and L. A. Pastur. Distribution of eigenvalues for some sets of random matrices. *Mathematics of the USSR-Sbornik*, 1(1):507–536, 1967.
- [46] Guionnet, Krishnapur, Manjunath, Zeitouni, and Ofer. The single ring theorem. *Annals of Mathematics*, 174(2):1189–1217, 2009.
- [47] Greg W. Anderson, Alice Guionnet, and Ofer Zeitouni. An introduction to random matrices. *Cambridge Studies in Advanced Mathematics*, 2009.
- [48] Terence Tao. *Topics in Random Matrix Theory*. American Mathematical Society,, 2012.
- [49] R Qiu and P Antonik. *Smart Grid and Big Data*. John Wiley and Sons, 2015.
- [50] Math HJ Bollen. *Understanding power quality problems*, volume 3. IEEE press New York, 2000.
- [51] Denis Hau Aik Lee. Voltage stability assessment using equivalent nodal analysis. *IEEE Transactions on Power Systems*, 31(1):454–463, 2016.
- [52] Goodarz Ghanavati, Paul DH Hines, and Taras I Lakoba. Identifying useful statistical indicators of proximity to instability in stochastic power systems. *IEEE Transactions on Power Systems*, 31(2):1360–1368, 2016.
- [53] Xinyi Xu, Xing He, Qian Ai, and Robert Caiming Qiu. A correlation analysis method for power systems based on random

- matrix theory. *IEEE Transactions on Smart Grid*, PP(99):1–10, 2015.
- [54] Rudolf Wegmann. The asymptotic eigenvalue-distribution for a certain class of random matrices. *Journal of Mathematical Analysis and Applications*, 56(1):113–132, 1976.
  - [55] Robert Caiming Qiu, Zhen Hu, Husheng Li, and Michael C Wicks. *Cognitive radio communication and networking: Principles and practice*. John Wiley & Sons, 2012.
  - [56] Yingshuang Cao, Long Cai, C Qiu, Jie Gu, Xing He, Qian Ai, and Zhijian Jin. A random matrix theoretical approach to early event detection using experimental data. *arXiv preprint arXiv:1503.08445*, 2015.
  - [57] M. L. Mehta. *Random matrices*, volume 142. Academic press, 2004.
  - [58] Z. Bai. Convergence rate of expected spectral distributions of large random matrices. part i. wigner matrices. *The Annals of Probability*, pages 625–648, 1993.
  - [59] Z. Bai, B. Miao, and J. Tsay. A note on the convergence rate of the spectral distributions of large random matrices. *Statistics & Probability Letters*, 34(1):95–101, 1997.
  - [60] F. Götze and A. Tikhomirov. Rate of convergence to the semi-circular law. *Probability Theory and Related Fields*, 127(2):228–276, 2003.
  - [61] Z. Bai, B. Miao, and J. Yao. Convergence rates of spectral distributions of large sample covariance matrices. *SIAM journal on matrix analysis and applications*, 25(1):105–127, 2003.
  - [62] V. L. Girko. Extended proof of the statement: Convergence rate of the expected spectral functions of symmetric random matrices  $\xi_n$  is equal to  $o(n^{1/2})$  and the method of critical steepest descent. *Random Operators and Stochastic Equations*, 10(3):253–300, 2002.
  - [63] Friedrich Götze and Alexander Tikhomirov. The rate of convergence for spectra of gue and lue matrix ensembles. *Open Mathematics*, 3(4):666–704, 2005.
  - [64] Voiculescu Dan. *Symmetries of some reduced free product  $C^*$ -algebras*. Springer Berlin Heidelberg, 1985.
  - [65] Voiculescu Dan. Limit laws for random matrices and free products. *Inventiones mathematicae*, 104(1):201–220, 1991.
  - [66] Serban Belinschi, Tobias Mai, and Roland Speicher. Analytic subordination theory of operator-valued free additive convolution and the solution of a general random matrix problem. *Journal Fr Die Reine Und Angewandte Mathematik*, 2013.
  - [67] Roland Speicher and Roland Speicher. Polynomials in asymptotically free random matrices. *Acta Physica Polonica*, 46(9), 2015.
  - [68] Greg W. Anderson. Convergence of the largest singular value of a polynomial in independent wigner matrices. *Annals of Probability*, 38(1):110C112, 2011.
  - [69] Zhidong Bai and Hewa Saranadasa. Effect of high dimension: by an example of a two sample problem. *Statistica Sinica*, pages 311–329, 1996.
  - [70] Zhidong Bai, Dandan Jiang, Jian-Feng Yao, and Shurong Zheng. Corrections to lrt on large-dimensional covariance matrix by rmt. *The Annals of Statistics*, pages 3822–3840, 2009.
  - [71] Olivier Ledoit and Michael Wolf. Some hypothesis tests for the covariance matrix when the dimension is large compared to the sample size. *Annals of Statistics*, pages 1081–1102, 2002.
  - [72] Song Xi Chen and Ying-Li Qin. A two-sample test for high-dimensional data with applications to gene-set testing. *The Annals of Statistics*, 38(2):808–835, 2010.
  - [73] Song Xi Chen, Li-Xin Zhang, and Ping-Shou Zhong. Tests for high-dimensional covariance matrices. *Journal of the American Statistical Association*, 2012.
  - [74] AJ Lee. *U-statistics. Theory and Practice,* Marcel Dekker, New York, 1990.
  - [75] US-Canada Power System Outage Task Force, Spencer Abraham, Herb Dhaliwal, R John Efford, Linda J Keen, Anne McLellan, John Manley, Kenneth Vollman, Nils J Diaz, Tom Ridge, et al. *Final report on the August 14, 2003 blackout in the United states and Canada: causes and recommendations*. US-Canada Power System Outage Task Force, 2004.
  - [76] Mica R Endsley. *Designing for situation awareness: An approach to user-centered design*. CRC Press, 2011.
  - [77] Mathaios Panteli, Peter Crossley, Daniel S Kirschen, Dejan J Sobajic, et al. Assessing the impact of insufficient situation awareness on power system operation. *Power Systems, IEEE Transactions on*, 28(3):2967–2977, 2013.
  - [78] Changchun Zhang and Robert C Qiu. Massive mimo as a big data system: Random matrix models and testbed. *IEEE Access*, 3:837–851, 2015.
  - [79] Mariya Shcherbina. Central limit theorem for linear eigenvalue statistics of the wigner and sample covariance random matrices. *ArXiv e-prints*, January 2011.
  - [80] Xing He, Qian Ai, Robert Caiming Qiu, and Wentao Huang. A big data architecture design for smart grids based on random matrix theory. *IEEE Transactions on Smart Grid*, 32(3):1, 2015.
  - [81] Jesper R Ipsen and Mario Kieburg. Weak commutation relations and eigenvalue statistics for products of rectangular random matrices. *Physical Review E*, 89(3), 2014. Art. ID 032106.
  - [82] Florent Benaych-Georges and Jean Rochet. Outliers in the single ring theorem. *Probability Theory and Related Fields*, pages 1–51, May 2015.
  - [83] Terence Tao. Outliers in the spectrum of iid matrices with bounded rank perturbations. *Probability Theory and Related*

- Fields, 155(1-2):231–263, 2013.
- [84] Xiaochen Zhang and Santiago Grijalva. A data-driven approach for detection and estimation of residential pv installations. IEEE Transactions on Smart Grid, 7(5):2477–2485, 2016.
  - [85] Xing He, Robert Caiming Qiu, Qian Ai, Lei Chu, Xinyi Xu, and Zenan Ling. Designing for situation awareness of future power grids: An indicator system based on linear eigenvalue statistics of large random matrices. IEEE Access, 4:3557–3568, 2016.
  - [86] Ray D Zimmerman and Carlos E Murillo-Snchez. Matpower 4.1 user’s manual. Power Systems Engineering Research Center, 2011.
  - [87] Robert Qiu and Michael Wicks. Cognitive networked sensing and big data. Springer, 2014.